Scientific Reports

https://doi.org/10.1038/s41598-026-56872-0

Article in Press

Artificial intelligence enabled performance evaluation of an enhanced SPR biosensor for malaria diagnosis

Received: 16 March 2026

Accepted: 3 June 2026

Published online: 08 June 2026

Cite this article as: Utshob M.A.A.I., Juwel M.B., Ishtiak K.M. *et al.* Artificial intelligence enabled performance evaluation of an enhanced SPR biosensor for malaria diagnosis. *Sci Rep* (2026). https://doi.org/10.1038/s41598-026-56872-0

Md. Al Amin Islam Utshob, Maymona Binte Juwel, Khandakar Mohammad Ishtiak, Aminur Rahman, M. M. Atiqur Rahman, Safayat-Al Imam, S. M. Ishraqul Huq & Quazi D. M. Khosru

Artificial Intelligence Enabled Performance Evaluation of an Enhanced SPR Biosensor for Malaria Diagnosis

[a]Md. Al Amin Islam Utshob, [a]Maymona Binte Juwel, [a]Khandakar Mohammad Ishtiak, [a]Aminur Rahman, [a]M. M. Atiqur Rahman, [a]Safayat-Al Imam, [a]S. M. Ishraqul Huq, [b,c*]Quazi D. M. Khosru

[a]Department of Electrical & Electronic Engineering, Ahsanullah University of Science and Technology, 141 & 142, Love Road, Tejgaon Industrial Area, Dhaka-1208, Bangladesh

[b]Department of Electrical and Electronic Engineering, Bangladesh University of Engineering and Technology, ECE Building, West Palashi Campus, Dhaka 1205, Bangladesh

[c]Prime University, 114/116 Mazar Road, Mirpur-1, Dhaka 1216, Bangladesh (On deputation from BUET)

*Corresponding Author Email: qdmkhosru@eee.buet.ac.bd

Abstract

Malaria remains a serious global health problem, particularly in areas where drug-resistant Plasmodium species and the expanded geographical distribution of malaria caused by climate change are of concern. In response to the pressing need for a rapid and highly sensitive malaria diagnostic method, this paper proposes a novel surface plasmon resonance (SPR) biosensor design with a multilayer N-FK51a+SiO_2+Cu+HfO_2+BP structure. The biosensor performance is analyzed using the transfer matrix method (TMM) and finite element method (FEM), and further verified by finite difference time domain (FDTD) simulations. The inclusion of SiO_2, Cu, HfO_2, and black phosphorus (BP) enhances the coupling, confinement, and interaction of the plasmonic field with the analyte. The biosensor design exhibits a maximum angular sensitivity of 541.42 deg/RIU, a narrow FWHM of 1.98 deg, a detection accuracy of 0.502 deg^{-1}, and a quality factor of 272.21 RIU^{-1}, which are outstanding, particularly for ring-stage malaria diagnosis. To further enhance the biosensor reliability, the sensor responses are modeled using ANN, ANFIS, and RBFNN models, which can predict the stages correctly. The comparative analysis proves the enhanced sensitivity and accuracy compared to the previously published SPR sensors and highlights the robustness of the sensor for real-time malaria diagnosis and broader biomedical application.

Keywords

Surface plasmon resonance, Hafnium oxide, FDTD, Malaria, RBFNN, pLDH

1. *Introduction*

Infectious diseases have had a great influence on human health, even surpassing the effects of war in terms of mortality and suffering, with malaria being one of the most severe. Malaria is a parasitic disease transmitted by the bite of infected female Anopheles mosquitoes and is a major global health concern, especially in developing countries. In developing countries, effective control and treatment of the disease are highly dependent on early, accurate, and specific diagnosis[1,2] . Conventional diagnosis, such as microscopic examination of blood smears and rapid diagnostic tests (RDTs), is hampered by some limitations, including decreased sensitivity at low levels of parasitemia, the need for trained personnel, long processing time, and high operational costs [3]. These challenges have driven increasing interest in the development of alternative diagnostic technologies that are cost-effective, highly sensitive, capable of real-time analysis, and suitable for large-scale application in resource-limited settings. Among emerging approaches, surface plasmon resonance (SPR) based biosensors have gained considerable attention. SPR biosensors enable label-free detection, provide real-time monitoring of biomolecular interactions, and offer high sensitivity at the nanoscale, making them well-suited for infectious disease diagnostics, including malaria detection [4,5] .

Surface plasmon resonance (SPR) operates through the excitation of surface plasmons, which are collective oscillations of free electrons generated at a metal-dielectric interface when illuminated by polarized light under appropriate conditions [6]. The resulting surface plasmon wave exhibits extreme sensitivity to variations in the local refractive index near the sensor surface, enabling the detection of biomolecular binding events in close proximity to the interface [7,8]. Changes in the plasmon resonance are commonly monitored using two principal interrogation techniques: angular interrogation, where the incident angle is varied at a constant wavelength, and wavelength interrogation, in which the excitation wavelength is scanned while maintaining a fixed incident angle [9]. A typical SPR sensor configuration comprises a high-refractive-index dielectric prism, most commonly BK7 glass, coated with a thin plasmonic metal layer such as gold (Au) or silver (Ag). Further dielectric layers or two-dimensional material layers are introduced to enhance the key performance parameters such as sensitivity, resonance quality, and stability [10]. Among the different methods of excitation, the Kretschmann configuration is the most popular one because of its high coupling efficiency, advantageous signal-to-noise ratio, and easy optical alignment [11]. Although there has been considerable progress in the development of SPR biosensors, the traditional design has been plagued by a number of issues. These include the lack of sensitivity when the concentration of the analyte is low, the effect of environmental fluctuations, the broad resonance curves that affect the accuracy of measurements, and the problem of material degradation, especially oxidation of silver films. Oxidation of silver surfaces causes a reduction in the plasmonic signal and a shortening of the sensor lifespan [12,13]. To address these challenges, there has been a recent emphasis on the design of SPR architectures with heterostructures made of plasmonic metals, semiconductors, and two-dimensional nanomaterials. These hybrid structures have improved plasmon field confinement, chemical stability, and optical properties, which have resulted in enhanced sensing performance [14–16] .

The research aims at the selective identification of malaria-specific biomarkers in the bloodstream during an active Plasmodium infection, with a special focus on parasite proteins used as reliable diagnostic markers. The main target biomarkers are Plasmodium lactate dehydrogenase (pLDH), histidine-rich protein 2 (HRP2), and other surface antigens, which have been extensively documented in the literature for their diagnostic accuracy and relevance [17]. The sensing mechanism leverages the unique binding interactions between the biomarkers and the designed biorecognition layers. These interactions cause localized changes in the refractive index at the metal-dielectric interface, resulting in detectable shifts in the surface plasmon resonance. The sensitivity of these resonance shifts is directly proportional to the concentration of the biomarkers, allowing for their sensitive, label-free, and real-time detection. The sensing mechanism offers a reliable and scalable solution for precise malaria detection, which satisfies the performance criteria of high-sensitivity applications [18].

In this work, a multilayer surface plasmon resonance biosensor with the N-FK51a+SiO_2+Cu+HfO_2+BP configuration is proposed for the detection of malaria at an excitation wavelength of 633 nm. The N-FK51a prism is employed as the coupling medium owing to its high RI, which helps to ensure the momentum matching between the incident p-polarized light and surface plasmons at the specified wavelength, thus ensuring a sharper resonance curve and higher excitation efficiency [19]. A thin layer of silicon dioxide (SiO_2) is added to the prism-metal interface to act as an optical spacer and adhesion layer, which helps to ensure a uniform deposition of the plasmonic film while reducing optical losses at the interfacial optical losses [20]. Copper (Cu) is chosen as the plasmonic material because of its strong plasmonic resonance in the visible spectrum at 633 nm, high electrical conductivity, and relative cost-effectiveness compared to noble metals [21]. However, the Cu sensitivity to oxidation and surface damage requires the addition of a protective dielectric layer to ensure long-term sensor functionality. In an effort to overcome these challenges and further improve the efficiency of the sensing process, a hafnium oxide (HfO_2) dielectric layer is added on top of the Cu layer. The high dielectric constant of HfO_2 ensures a stronger confinement of the electromagnetic field at the sensing interface, in addition to its role as a diffusion barrier that improves chemical and environmental stability [22]. The outermost sensing layer is made of black phosphorus (BP), a two-dimensional nanomaterial that has a direct bandgap, high carrier mobility, and large surface-to-volume ratio [23]. P increases biomolecule adsorption and the local refractive index change upon binding of the analyte molecules, resulting in a sharper resonance shift [24]. The synergistic effect between the Cu plasmonic layer, HfO_2 dielectric spacer, and BP sensing interface greatly enhances the coupling between plasmons and the analyte, making the proposed architecture amenable for the detection of early-stage malaria biomarkers. In addition, the compatibility of all layers with standard thin-film processing techniques makes the proposed architecture amenable for cost-effective sensor development.

In the recent past, machine learning (ML) approaches have received considerable attention in various fields of science and engineering for their ability to effectively model complex systems [25]. In the optical and photonics research community, ML algorithms have been identified as useful tools for dealing with the computational challenges involved in traditional numerical methods [26]. Through the learning of complex nonlinear relationships between input parameters and system responses from labeled datasets, supervised ML models facilitate fast and accurate predictions of device performance for novel conditions [27]. This feature is especially useful in the design and optimization of optical biosensors, in which conventional simulation-driven methods tend to require large computational efforts. In the case of surface plasmon resonance (SPR) biosensors, ML platforms have shown great potential in exploring large parameter spaces to determine optimal sensing conditions with improved sensitivity and selectivity. Of the supervised learning methods, Artificial Neural Networks (ANN), Adaptive Neuro-Fuzzy Inference Systems (ANFIS), and Radial Basis Function Neural Networks (RBFNN) are especially useful owing to their robustness, high approximation capabilities, and ability to simulate complex nonlinear optical responses [28,29]. In this study, an ML-based SPR biosensing system is proposed for malaria diagnosis by leveraging the RI differences caused by red blood cells (RBCs) at various stages of infection. The proposed sensor utilizes the unique refractive indices of RBCs for normal (1.402), ring (1.395), trophozoite (1.381), and schizont (1.371) stages to facilitate accurate stage-wise diagnosis [30,31].

The contributions of innovation in this research work involve the development of an SPR Biosensor with multiple layers and AI assistance. As compared to the usual SPR biosensors, the present study utilizes a novel N-FK51a+SiO_2+Cu+HfO_2+BP multilayer, with each material used in the layer being selected such that it enhances the coupling efficiency, confining of the electromagnetic field, and sensing stability. In this respect, the present device outperforms other malaria SPR biosensors in terms of its angular sensitivity. In addition to that, the new methodology focuses on the identification of malaria biomarkers like pLDH and HRP2, thereby making it possible to distinguish between the various stages of malaria based on the refractive index changes. The application of such a high-performing plasmonic design along with machine learning approaches (ANN, ANFIS, and RBFNN) does not only enhance the sensitivity of the sensors but also ensures improved accuracy in predicting the various stages of malaria infection.

2. Methods & Design Principles

For the analysis of the proposed SPR biosensor, extensive electromagnetic simulations were performed using three well-established numerical methods: the Transfer Matrix Method (TMM), Finite Difference Time Domain (FDTD), and Finite Element Method (FEM). The main approach to be used in the course of the current analysis is the transfer matrix method, TMM, which is characterized by exceptional efficiency and precision, especially when considering such properties as reflection and resonant angle values at the SPR effect. When compared to the complete numerical algorithms like FEM, TMM is distinguished by low requirements for computer resources but still allows achieving quite acceptable accuracy in calculations. In order to confirm the validity of the results, two other numerical algorithms have been applied including FEM and Finite Difference Time Domain (FDTD) methods. The TMM was employed to calculate the reflectance spectra and the resonance angles of the multilayer structure for p-polarized light at 633 nm [32]. FDTD analyses were carried out to analyze the time-dependent propagation of electromagnetic waves and the behavior of surface plasmon excitation. In addition, modeling was done using FEM to provide information on the electric field distributions and the field confinement at the sensing interface. This ensured that the resonance characteristics, reflectance minima, and overall sensing performance [33]. An optimization approach using machine learning was adopted. A vast dataset was created by varying the RI and thickness of the layers. Once preprocessing was done, the data was used to train and test the ANN, ANFIS, and RBFNN models for the prediction of resonance angle and sensitivity. The best model was chosen based on its predictive ability and robustness, and the results were verified using independent simulation results. This comprehensive computational model enhances efficiency and enables accurate, stage-wise malaria detection.

2.1 Structural Modelling

The proposed SPR biosensor for malaria diagnosis consists of six functional layers in a Kretschmann arrangement, which are an N-FK51a prism, a SiO_2 adhesive layer, a Cu plasmonic film, a HfO_2 dielectric spacer, a black phosphorus (BP) protective layer, and the surrounding analyte medium. The Kretschmann arrangement is used in the SPR biosensor because of its high coupling efficiency, ease of alignment, and ability to control the parameters. In this configuration, the N-FK51a prism serves as the coupling element and directs p-polarized incident light of wavelength λ = 633 nm toward the sensing interface. The RI of the N-FK51a glass prism is determined by the wavelength of the light incident [19],

$$n_p(\lambda) = \sqrt{1 + \frac{a_1\lambda^2}{\lambda^2 - b_1} + \frac{a_2\lambda^2}{\lambda^2 - b_2} + \frac{a_3\lambda^2}{\lambda^2 - b_3}} \quad (1$$

Where a_i and b_i are the Sellmeier coefficients which are given as a_1= 0.971247817, a_2= 0.216901417, a_3= =0.904651666, b_1 =0.00472301995, b_2= 0.0153575612, b_2= 168.68133, and λ is the wavelength of the incident light (µm). Between the prism and the plasmonic Cu film in the proposed multilayer structure, SiO_2 (RI=1.4636+0.0016623i) serving as a protective and adhesion layer [34]. SiO_2 enhances the bond strength between the prism surface and the metallic layer, thereby enhancing overall sensor stability. It also helps in minimizing surface roughness, which are essential for the highly effective excitation of surface plasmons.

A Cu metal layer is deposited on the top of the adhesion layer. The RI of Cu is calculated using the Drude-Lorentz model, as illustrated below [35],

$$n_{Cu} = (\varepsilon_r + i\varepsilon_i)^{\frac{1}{2}} = \left(1 - \frac{\lambda^2 \lambda_{cw}}{\lambda_{pw}(\lambda_{cw} + i\lambda)}\right)^{\frac{1}{2}} \quad (2)$$

For Cu, the collision (λ_{cw}) and plasma wave (λ_{pw}) wavelengths are 4.0852×10^{-5} m and 1.3617×10^{-7}m respectively. Hafnium oxide (HfO_2) is incorporated into the proposed sensor architecture due to its high chemical stability, large dielectric constant, and strong resistance to environmental degradation, making it suitable for reliable SPR operation. The RI of the HfO_2 layer is taken as 1.91, which contributes to enhanced electromagnetic field confinement at the metal-dielectric interface and improves the overall sensitivity of the sensor by amplifying its response to small RI variations in the sensing medium [36]. In addition, the resonance properties of the SPR sensor can be properly adjusted by changing the thickness of the HfO_2 layer, which helps to control the resonance position and the sharpness of the dip. The dielectric layer not only helps to improve the sensing performance but also serves as a protective layer for the plasmonic film. The BP layer is positioned at the top of the structure and has a RI of 3.5+0.01i [37]. The high carrier mobility of BP, together with its pronounced in-plane anisotropy, makes it especially suitable for light-matter interactions, which determine the overall resonance shifts, overshadowing minor variations in the RI [38]. Moreover, its atomically flat surface is readily functionalized, serving as an ideal substrate for the targeted immobilization of chemical sensors. Table 1 represents the refractive indices and thickness of all the involved layers in the proposed SPR configuration.

Table 1. Optimized Layer Thickness and RI Parameters of the Proposed Structure

Materials	Refractive Index (RI)	Thickness (nm)
N-FK51a prism	1.4853	-
SiO_2	1.4636+0.0016623i	20
Cu	0.0369+4.5393i	50
HfO_2	1.91	2
BP	3.5+0.01i	0.53

2.2 Mathematical Modelling

Prism coupling is one of the most frequently employed methods for excitation of surface plasmons (SPs) in the Kretschmann configuration. This method offers precise control over experimental parameters and conditions, as well as straightforward alignment [39]. In this configuration, resonant excitation is facilitated by the interaction of a transversely magnetic (TM) polarized light beam with the metal-dielectric interface at a specific incidence angle and wavelength. Resonance happens when the propagation constant of the incident light (K_{light}) is equivalent to the surface plasmon wavevector (β_{SP}). Consequently, the resonance condition for the prism coupling configuration can be expressed as [40]:

$$K_{light} = \beta_{SP} \quad (3)$$

$$\frac{2\pi}{\lambda} n_p \sin(\theta_i) = \frac{2\pi}{\lambda} \mathrm{Re}\left\{\sqrt{\frac{\varepsilon_m \varepsilon_d}{\varepsilon_m + \varepsilon_d}}\right\} \quad (4)$$

Here, n_p and λ denote the RI of the prism and the wavelength of the incident light, respectively. θ_i denotes the angle of incidence, while ε_m, ε_d represents the real part of the dielectric parameter associated with the metal. The angle of incidence for SPR can be determined using the following equation [40]:

$$\theta_i = \sin^{-1}\left[\left(\frac{1}{n_p}\right) \mathrm{Re}\left\{\sqrt{\frac{\varepsilon_m \varepsilon_d}{\varepsilon_m + \varepsilon_d}}\right\}\right]$$

Angular modulation is used to study the functions of the proposed multilayer structure. The reflectance of p-polarized incident light is calculated by the Transfer Matrix Method (TMM) based on Fresnel multilayer reflection theory to obtain its optical response [41]. The characteristic surface plasmon resonance curve is generated by the variation of the total reflected intensity (R_p) as a function of the incidence angle (θ). The mathematical expressions for the total reflectivity (R_p) and the reflection coefficient (q_p) are as follows [42]:

$$R_p = q_p q_p^* = |q_p|^2 \quad (6)$$

$$q_p = \frac{(M_{11} + M_{12} n_N) - (M_{21} + M_{22} n_N)}{(M_{11} + M_{12} n_N) + (M_{21} + M_{22} n_N)}$$

Here, M denotes the characteristics matrix of the SPR sensor [43]. The transverse RI and attributes matrix are delineated as follows [44],

$$n_k = \sqrt{\left(\left[\frac{\mu_k}{\varepsilon_k}\right]\right)}\cos\theta_k = \sqrt{\frac{\varepsilon_k - (n_p \sin\theta)^2}{\varepsilon_k^2}} \quad (8)$$

$$M_{if} = \left[\prod_{K=2}^{N-1} \begin{pmatrix} \cos\beta_k & -i\sin\beta_k \\ -in_k \sin\beta_k & \cos\beta_k \end{pmatrix}\right]_{if} = \begin{bmatrix} M_{11} & M_{12} \\ M_{21} & M_{22} \end{bmatrix} \quad (9)$$

Furthermore, the equations determine the arbitrary stage constant (β_k) and wave impedance (z_k) for the k^{th} stratum [45],

$$\beta_k = \frac{2\pi}{\lambda} n_k \cos\theta_k (z_k - z_{k-1}) = \frac{2\pi}{\lambda} d_k \sqrt{\varepsilon_k - (n_p \sin\theta)^2} \quad (10)$$

$$z_k = \frac{k_x n_k \cos\theta_k}{\left(2\pi c/\lambda_{inc}\right)\varepsilon_k^2} \quad (11)$$

Where, d_k and ε_k are the thickness and permittivity associated with k^{th} stratum, respectively. And for the k^{th} stratum, polar input angle θ_k is given by [42]:

$$\theta_k = \frac{1}{\cos\left(\sqrt{1 - \left(n_{k-1}/n_k\right)(\sin\theta)^2}\right)}$$

2.3 Optical Properties and Material Compatibility of the Proposed SPR Sensor

To validate the 1D TMM results, a detailed Finite Element Method (FEM) analysis was performed for the proposed N-FK51a+SiO_2+Cu+HfO_2+BP malaria biosensor. Fig. 1(a) shows the mesh configuration of the multilayer structure, carefully refined near the interfaces to accurately capture the strong electromagnetic field variations. Fig. 1(b) illustrates the two-dimensional electric field distribution (V/m) at the resonance angle of 87.51 deg. A strong field enhancement is noticed at the Cu+HfO_2+BP sensing interface, where the electric field strength is found to be around 476 kV/m. The strong localization at the metal-analyte interface is a clear indication of the efficient generation of the surface plasmon polaritons. The field strength is noticed to decay exponentially into the metal and the analyte, as seen in the case of plasmonic modes. The total electric field distribution, as shown in Fig. 1(c), is computed using the equation as $E_{total} = \sqrt{E_x^2 + E_y^2}$ [18]. where E_x and E_y are the lateral and normal electric field components, respectively. The tight confinement of the E_{total} field at the outer sensing interface confirms the strong light-analyte interaction, which directly affects the RI sensitivity. Fig. 1(d) shows the three-dimensional representation of the z-component of the electric field at 87.51 deg, represented as a height profile. The peaks and troughs in the 3D representation confirm the stable propagation of SPP at the Cu dielectric interface. The optimized thickness values of the SiO_2, Cu, HfO_2, and BP layers are used to maximize the electric field confinement and resonance, which further improves the angular detection sensitivity of the proposed malaria biosensor.

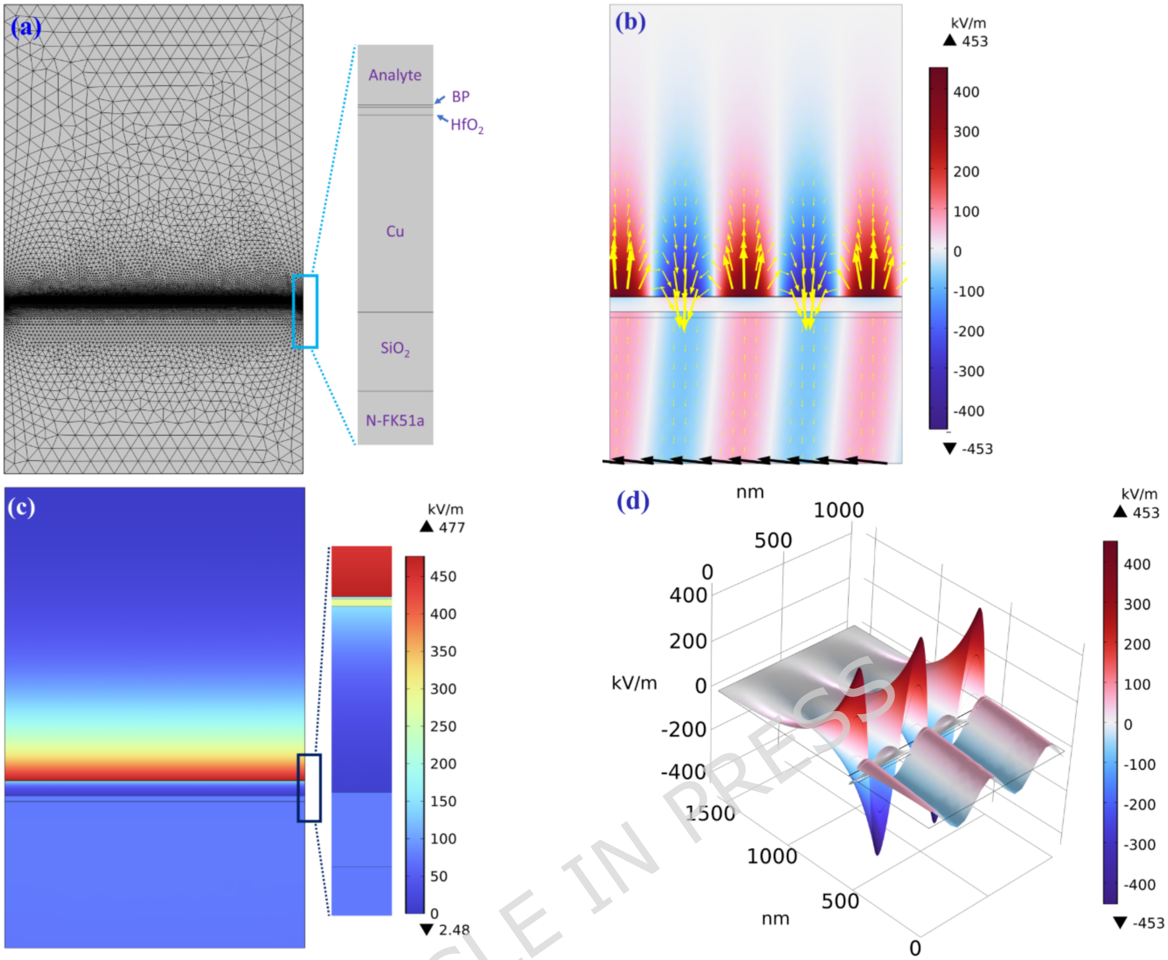

Fig. 1 (a) Mesh view of the proposed structure, (b) 2D electric field distribution (V/m) at an angle of resonance of 87.51 deg, (c) Total electric field $\left(\sqrt{E_x^2 + E_y^2}\right)$, and (d) 3D view of the z component of the electric field (V/m) as it moves at an angle of resonance of 87.51 deg, as viewed from the height surface.

2.4SPR performance metrics

One key criterion for the performance measurement of SPR biosensors is the sensitivity (S). Sensitivity is given by the ratio of the change in RI (Δn) and the variation of the resonance angle ($\Delta\theta_{res}$) with respect to the respect. Sensitivity is also expressed as [46,47]:

$$S = \frac{\Delta\theta_{res}}{\Delta n} \text{(in deg/RIU)} \qquad (13)$$

There are several other key parameters which have to be considered to estimate the overall efficiency of SPR sensors. Detection Accuracy (DA), Quality Factor (QF), Minimum reflectance (R_{min}), Full Width at Half Maximum (FWHM), and Figure of Merit (FOM) are commonly being used to test the efficiency of SPR sensors. Below is a description of these parameters [48,49]:

$$FWHM = \theta_{max} - \theta_{min} (deg) \quad (14)$$

$$QF = \frac{S}{FWHM} (\text{in } RIU^{-1})$$

$$DA = \frac{1}{FWHM} (deg^{-1})$$

$$FOM = S \times \frac{1 - R_{min}}{FWHM}$$

2.5 Possible Fabrication Techniques

The possible fabrication procedure of the proposed N-FK51a+SiO_2+Cu+HfO_2+BP multilayer structure is schematically illustrated in Fig. 2. An optical-grade N-FK51a prism was first used as the substrate and thoroughly cleaned using sequential ultrasonic treatment in acetone, isopropanol, and deionized water, followed by nitrogen drying to ensure a contaminant-free surface. A thin SiO_2 buffer layer was subsequently deposited onto the prism surface by thermal evaporation under high-vacuum conditions to promote adhesion, improve interfacial stability, and provide optical index matching [50]. Subsequently, a thin film of Cu was deposited on top of the SiO_2 layer using an epitaxial deposition method to achieve a smooth, highly crystalline metallic film with favorable properties for efficient plasmon excitation [51]. The Cu film thickness was precisely controlled to maximize the optical response of the structure. To prevent damage to the metal surface and maximize field confinement, a conformal layer of HfO_2 dielectric material was deposited on top of the Cu film using atomic layer deposition (ALD), which allowed for thickness control at the atomic scale [52]. Finally, a layer of BP was grown on top of the HfO_2 surface using a mechanical exfoliation and dry transfer method, which was conducted in controlled conditions to prevent environmental degradation [53]. The deposition method ensures a high-quality interface, uniformity in structure, and optimal optical properties for sensing. In terms of practical realization, the fabricated N-FK51a+SiO_2+Cu+HfO_2+BP nanocomposite can be easily fabricated using conventional thin-film deposition technology. Both SiO_2 and Cu can be deposited using the technique of thermal evaporation, while HfO_2 can be accurately fabricated using atomic layer deposition. Meanwhile, the BP can be transferred using the existing dry-transfer technique to avoid any damage to the material. In addition, according to the fabrication tolerance analysis described above, it is clearly shown that the sensitivity remains stable with ±10% variations in thickness for the biosensor fabricated by the proposed structure.

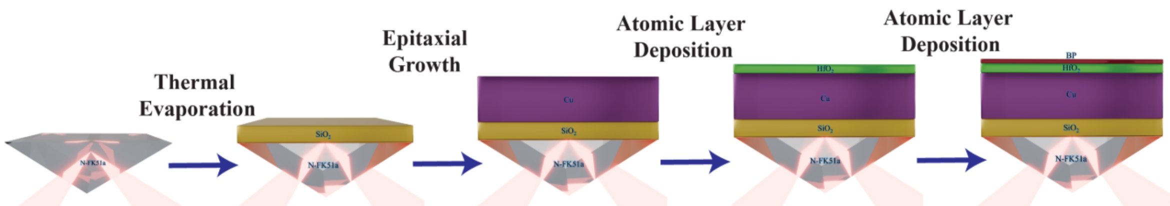

Fig. 2 Step by step fabrication methods for the proposed SPR sensor.

3. Result and Analysis

3.1 Developing the proposed Sensor

The designed biosensor has been developed with optimized geometric patterns corresponding to the three phases of the malaria disease, ensuring variations in reflectance based on the angle of incidence. The sensing layer has been optimized with a customized material composition to ensure high sensitivity to blood components and accurate discrimination among the different phases of the malaria disease. Fig. 3 shows the reflectance intensity profiles for different stages of a malaria infection, and a comparative analysis of different SPR sensor designs. The basic design (Fig. 3a) showed no sensing capability, with a sensitivity of 0 deg/RIU, a QF of 0 RIU^{-1}, and a DA of 0 deg^{-1}. After adding a Cu layer (Fig. 3b), the sensing capability was significantly enhanced, with a sensitivity of 286.28 deg/RIU, a DA of 0.706 deg^{-1}, and a QF of 202.17 RIU^{-1}. Further enhancement was observed after introducing a HfO_2 layer (Fig. 3c), which increased the angular sensitivity to 375.71 deg/RIU, with a DA of 0.594 deg^{-1} and a QF of 223.24 RIU^{-1} .The fully optimized configuration (Fig. 3d) exhibited the highest sensing performance, attaining a maximum angular sensitivity of 541.42 deg/RIU and a QF of 272.21 RIU^{-1} for the ring stage of malaria infection, thereby confirming that systematic structural refinement significantly enhances plasmonic response and overall sensor efficiency in Table 2.

Table 2. Performance metrics of the development malaria stages of SPR biosensor

Configuration	Sensitivity (deg/RIU)	R_{min}	QF (RIU^{-1})	DA (deg^{-1})
N-FK51a+SiO_2	-	-	-	-
N-FK51a+SiO_2+Cu	286.28	0.065	202.17	0.706
N-FK51a+SiO_2+Cu+HfO_2	375.71	0.037	223.24	0.594
N-FK51a+SiO_2+Cu+HfO_2+BP	541.42	0.011	272.21	0.502

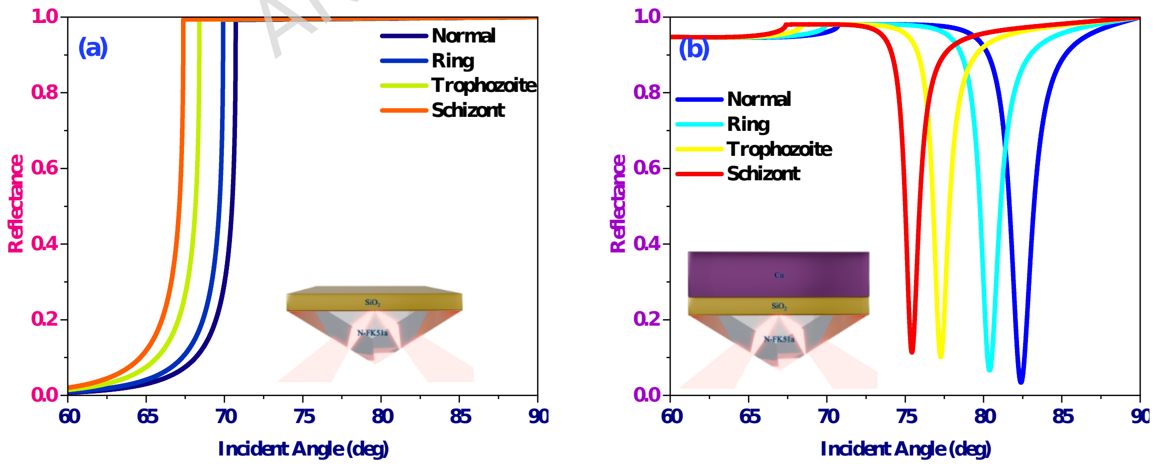

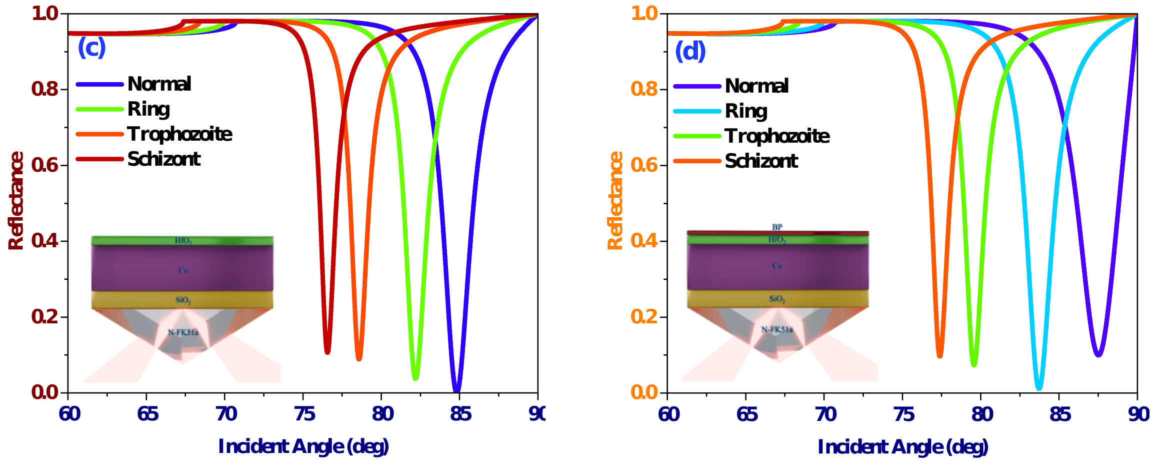

Fig. 3 Reflectance vs Incident angle (deg) curve (a) N-FK51a+SiO_2, (b) N-FK51a+SiO_2+Cu, (c) N-FK51a+SiO_2+Cu+HfO_2 , and (d) N-FK51a+SiO_2+Cu+HfO_2+BP.

3.2 Impact of choosing prism

A systematic comparison of different coupling prism materials clearly demonstrates in Fig. 4 that the N-FK51a prism provides the most favorable performance for the proposed SPR biosensor. When N-FK51a is employed, the sensor exhibits remarkably high sensitivities of 541.42, 378.19, and 326.48 deg/RIU for the ring, trophozoite, and schizont stages, respectively. These high sensitivities are accompanied by consistently large QF values of 272.21, 251.28, and 247.33 RIU^{-1}, confirming the formation of sharp resonance dips and excellent signal fidelity across all stages of malaria infection. In contrast, the remaining prism materials show significantly inferior resonance characteristics even when evaluated at a representative stage. For the ring stage, BK1 prism yield relatively low sensitivity of 127.85 deg/RIU and DA of 1.005 deg^{-1}, along with broader resonance width of 0.995 deg and limited FOM of 110.68, indicating weak plasmon excitation. Similarly, SF5 and BAF10 have relatively poorer performance metrics, with sensitivities of 87.57 and 88 deg/RIU, resonance widths of 0.704 and 0.707 deg, and relatively low FOM values of 107.53 and 107.58, indicating a lack of sufficient RI contrast for efficient surface plasmon resonance coupling. While BK7 has relatively better performance metrics than the other conventional prisms, with sensitivities of 204.71, 186.61, and 176.8 deg/RIU and FOM values of 133.24, 138.46, and 143.32 for the ring, trophozoite, and schizont stages, respectively, its resonance is still much broader and less sensitive than that of N-FK51a. The superior performance of the N-FK51a prism arises from its optimal RI, which enables efficient momentum matching between the incident optical field and surface plasmons, leading to stronger plasmon excitation, lower R_{min}, narrower resonance width, and enhanced resonance quality. Consequently, N-FK51a is identified as the most suitable coupling prism for achieving high sensitivity, sharp resonance characteristics, and reliable malaria detection in the proposed SPR biosensor.

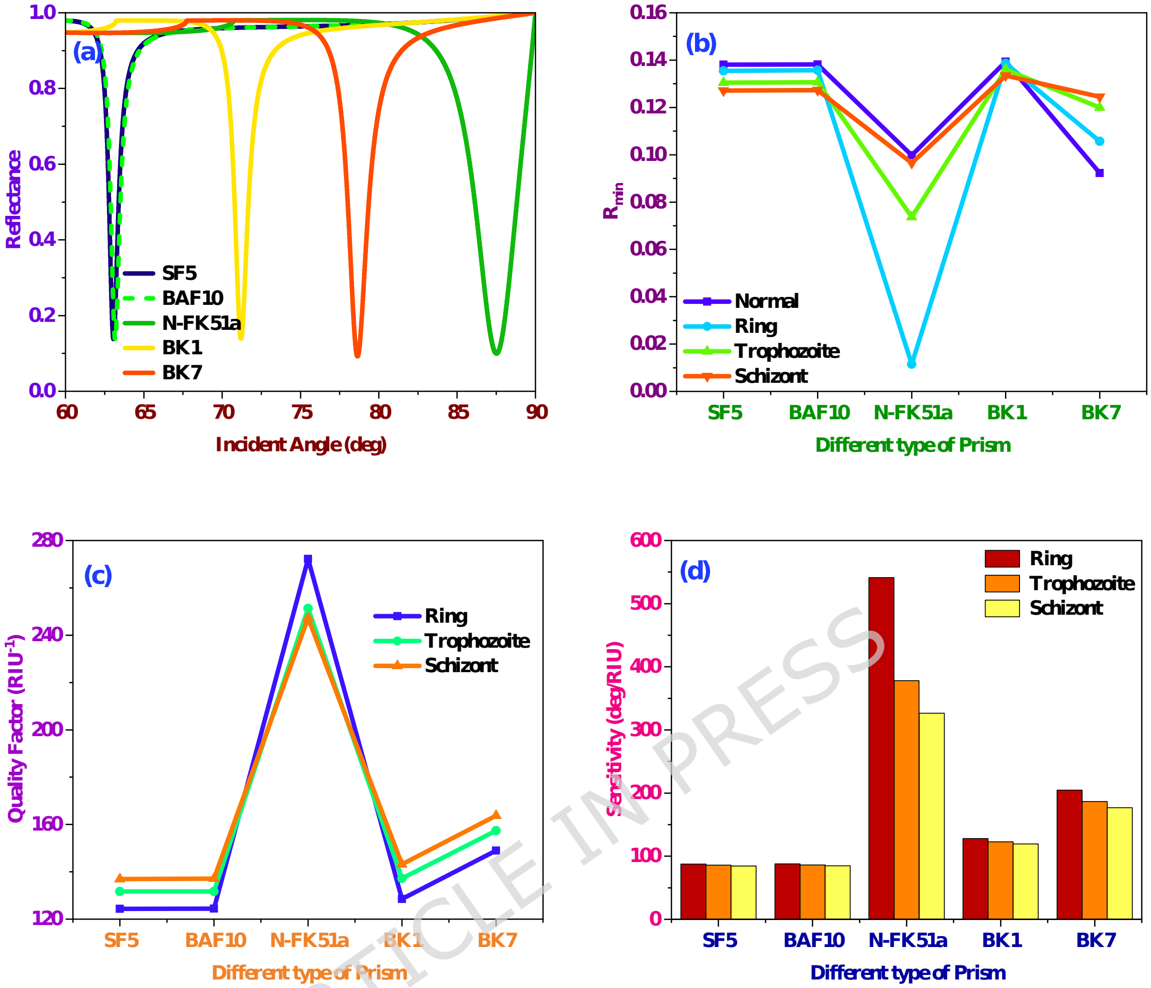

Fig. 4 Performance analysis using different prism: (a) Reflectance vs Incident angle (Normal Stage), (b) R_{min}, (c) QF, and (d) Sensitivity.

3.3 Impact of adhesive layer

The effect of SiO_2 layer thickness on the performance of the proposed SPR biosensor was systematically investigated, as summarized in Fig. 5, by varying the thickness from 0 nm to 100 nm while keeping all other layers unchanged. At 0 nm thickness, although the sensor exhibits relatively high sensitivity values are 549, 381.95 and 329.19 deg/RIU for the ring trophozoite and schizont stage, this condition is accompanied by a comparatively high R_{min}, a broad resonance width of 1.94, 1.46, and 1.29 deg for ring, trophozoite, and schizont stages, and an inflated QF that compromises resonance stability and DA. When the SiO_2 thickness is increased to 20 nm, the sensor demonstrates a well-balanced performance, achieving high sensitivities of 541.43, 378.19, and 326.48 deg/RIU, together with low R_{min} of 0.011, 0.073 and 0.096, narrow resonance widths of approximately 1.98, 1.50, and 1.32 deg, and high FOM values are 269.08, 232.76 and 223.46 for the ring, trophozoite, and schizont stages. Conversely, for thickness values above 20 nm, the sensing performance starts degrading gradually. For thickness values of 40 nm and 60 nm, the sensitivity starts dropping below 532.85 and 524.42 deg/RIU for the ring stage, and the resonance width starts increasing above 2.02 and 2.06 deg, respectively. For even higher thickness values of 80 nm and 100 nm, the sensitivity starts dropping below 515.85 and 507.42 deg/RIU, with increased R_{min} values, and increased resonance widths above 2.09 and 2.12 deg, and decreased QF values of 245.88 and 238.56 RIU-1 for ring stage. The reason for this degradation is excessive dielectric spacing, which weakens evanescent field penetration and reduces effective momentum matching between the incident light and surface plasmons. Consequently, the optimal value of SiO_2 thickness is determined to be 20 nm, which provides the best possible combination of efficient plasmon excitation, low reflectance loss, sharp resonance features, and high resolution for accurate malaria detection at all stages.

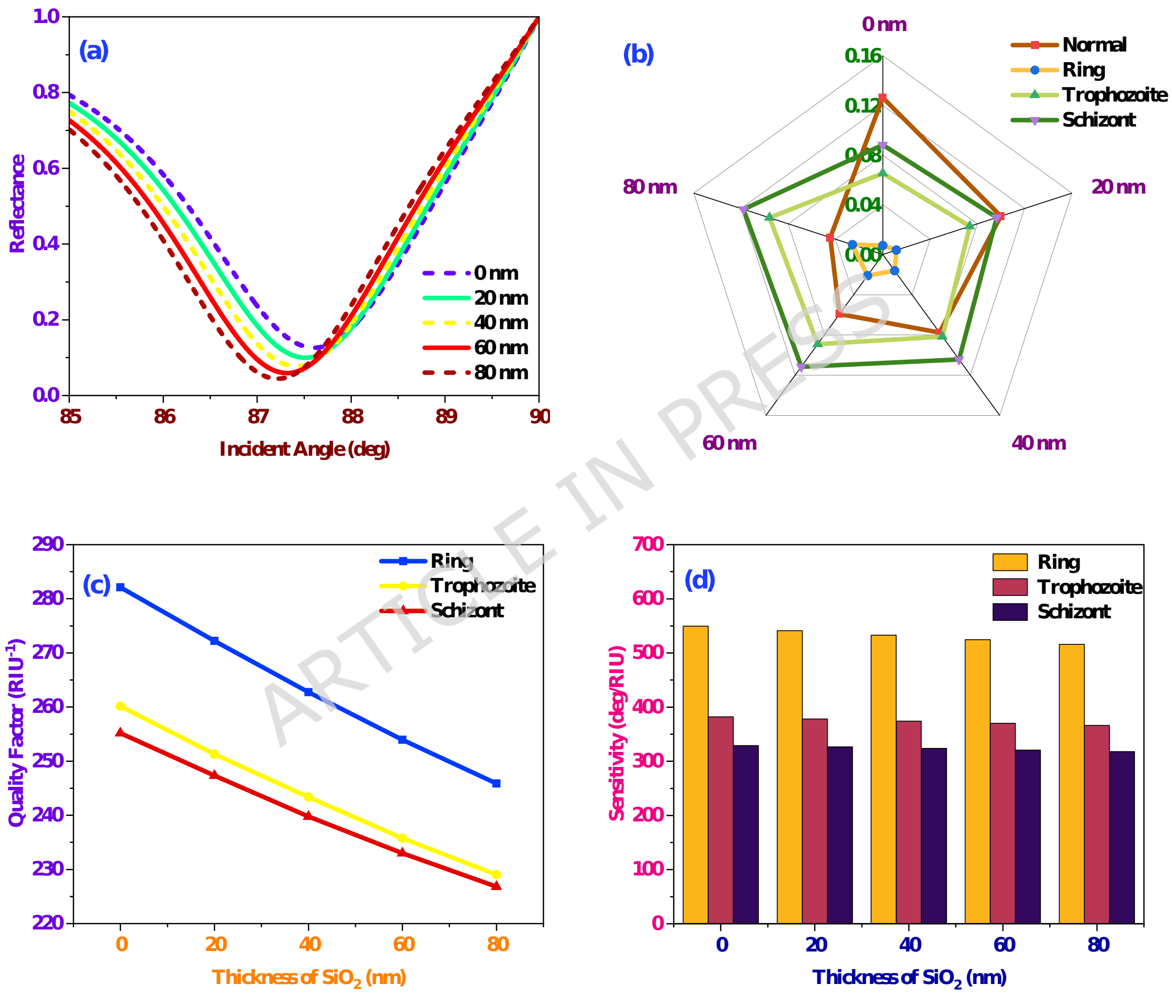

Fig. 5 Thickness variation of adhesive layer: (a) Reflectance vs Incident angle (Normal Stage), (b) R_{min}, (c) QF, and (d) Sensitivity.

3.4 Impact of plasmonic layer

The impact of Cu layer thickness on the proposed SPR biosensor performance was examined by varying the thickness from 40 nm to 60 nm, as shown in Table 3. At a Cu thickness of 40 nm, the sensor exhibits sensitivities of 386, 300.81, and 268.81 deg/RIU for the ring, trophozoite, and schizont stages, respectively. However, the corresponding R_{min} values remain high at 0.337, 0.428, and 0.451, indicating weak plasmon excitation and poor resonance depth. When the thickness is increased to 45 nm, sensitivity improves to 463.71, 341.05, and 299.16 deg/RIU, yet the R_{min} values still exceed the desired limit which is 0.1, remaining at 0.132, 0.234, and 0.262 for the three stages. Conversely, for a Cu thickness of 50 nm, the sensor exhibits a balanced and excellent performance with high sensitivities of 541.43, 378.19, and 326.48 deg/RIU with very low R_{min} values of 0.011, 0.073, and 0.096 for the ring, trophozoite, and schizont stages, respectively. These values are persistently below 0.1, indicating a high level of plasmon coupling and efficient field transfer at the metal-dielectric interface. For increased thicknesses of 55 nm and 60 nm, while the sensitivities continue to rise to above 588.42 and 583.71 deg/RIU for the ring stages, the R_{min} values again exceed the acceptable limit for ring stage, along with wider resonance curves and lower sensing accuracy. This is due to an increased metal thickness that causes increased damping and reduced effective field penetration into the sensing area. From Fig. 6, a Cu thickness of 50 nm is chosen as the best option, as it is the only choice that ensures low R_{min} for all stages of malaria infection, besides providing high sensitivity, sharp resonance curves, and accurate sensing performance.

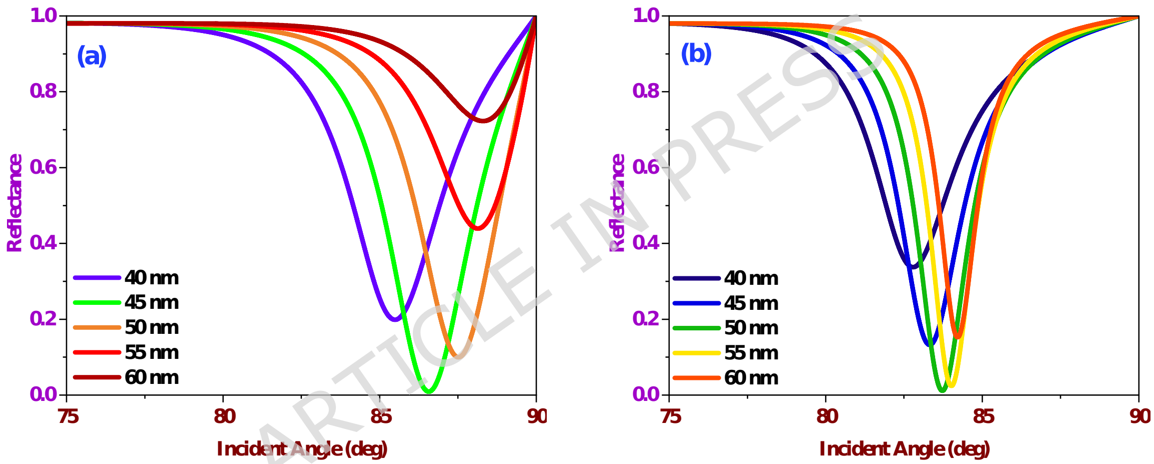

Fig. 6 Reflectance vs Incident angle for thickness variation of Cu (a) Normal stage, and (b) Ring Stage.

Table 3. Performance metrics for varying different Cu thickness

Thickness of Cu layer (nm)	Malaria Stages	Sensitivity (deg/RIU)	R_{min}	DA (deg^{-1})	QF (RIU^{-1})	FOM	FWHM (deg)
40	Ring	386	0.337	0.316	122.30	81.04	3.15
	Trophozoite	300.80	0.428	0.364	109.50	62.63	2.74
	Schizont	268.80	0.451	0.396	106.50	58.38	2.52
45	Ring	463.71	0.132	0.407	188.73	163.76	2.45
	Trophozoite	341.04	0.234	0.500	170.52	130.59	2.00
	Schizont	299.16	0.262	0.557	166.66	122.87	1.79
	Ring	**541.42**	**0.011**	**0.502**	**272.21**	**269.08**	**1.98**

50	**Trophozoite**	**378.19**	**0.073**	**0.664**	**251.28**	**232.76**	**1.50**
	Schizont	**326.48**	**0.096**	**0.757**	**247.33**	**223.46**	**1.32**
	Ring	588.42	0.024	0.592	348.80	340.38	1.68
55	Trophozoite	402.14	0.001	0.846	340.22	339.85	1.18
	Schizont	344.22	0.006	0.982	338.13	336.02	1.01
	Ring	583.71	0.152	0.667	389.66	330.19	1.49
60	Trophozoite	406.38	0.042	1.023	415.94	398.29	0.97
	Schizont	348.09	0.025	1.212	421.93	411.26	0.82

3.5 Strategic selection and thickness optimization of dielectric layers

A comparative analysis was conducted to determine the most appropriate oxide thickness for multi-stage malaria detection using the proposed SPR biosensor. As shown in Fig. 7, five dielectric materials, such as $BaTiO_3$, Al_2O_3, MgO, Li_3BO_5, and HfO_2, were compared based on sensitivity, DA, and FOM for the ring, trophozoite, and schizont stages. The BaTiO3-based design showed moderate sensitivity (334.28, 347.95, and 312.09 deg/RIU) with relatively lower FOM. Al_2O_3 and MgO showed better performance with a maximum sensitivity of about 466 and 449.42 deg/RIU for the ring stage, respectively, along with higher DA and FOM. Li_3BO_5 showed balanced but relatively lower sensitivity (385.71, 302.19, and 270.09 deg/RIU). Among all the candidates, the HfO_2 layer showed the highest and most stable performance with a maximum sensitivity of about 541.42, 378.19, and 326.48 deg/RIU for the ring, trophozoite, and schizont stages, respectively, along with higher FOM (269.08, 232.76, and 223.46). The main reason for this improved performance is the higher RI of HfO_2, which enhances the confinement of the electromagnetic field and further improves the plasmonic coupling between the metal and dielectric layers in contact with the analyte.

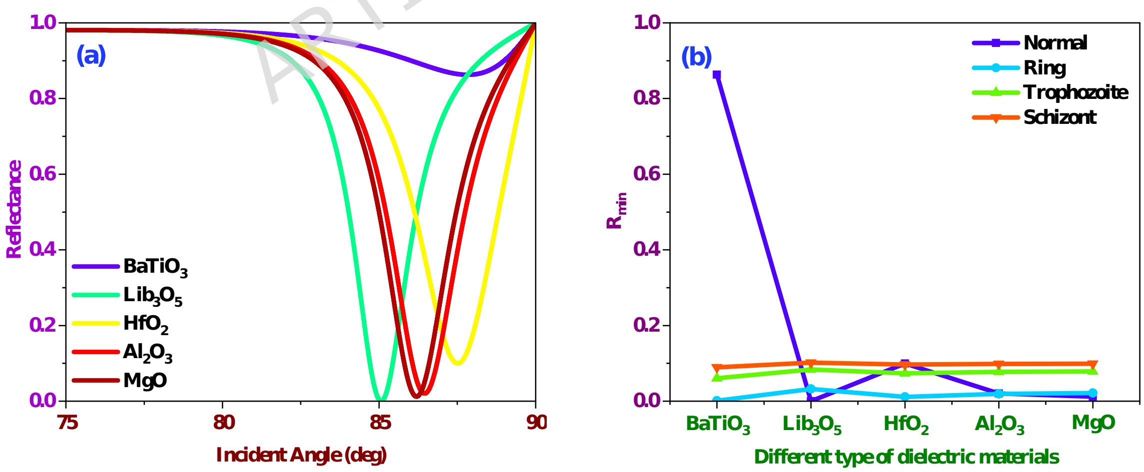

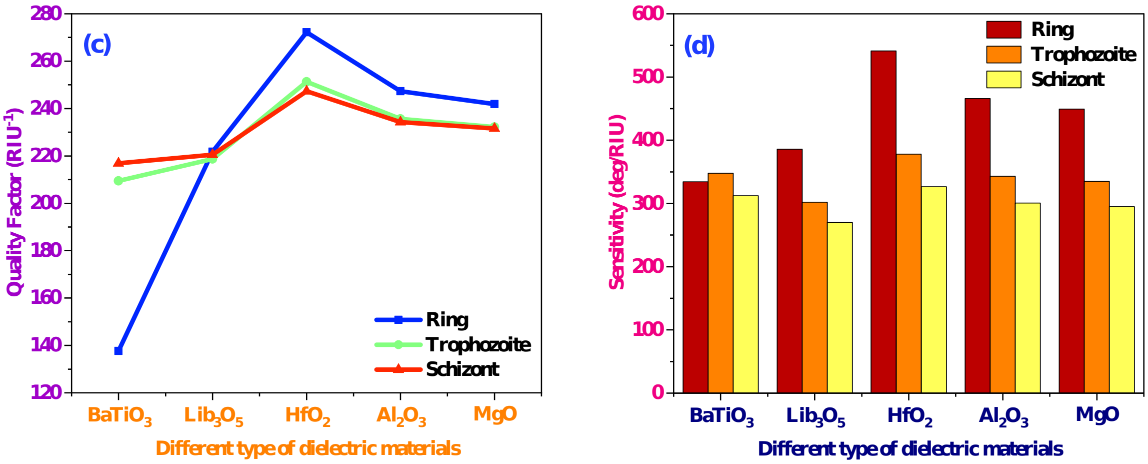

Fig. 7 Performance analysis using different dielectric layer: (a) Reflectance vs Incident angle (Normal Stage), (b) R_{min}, (c) QF, and (d) Sensitivity.

After material choice, the thickness of the HfO_2 layer was optimized from 1 nm to 3 nm systematically, as shown in Fig. 8. For a thickness of 1 nm, the sensor had relatively lower sensitivities (402.85, 311.76, and 277.51 deg/RIU) and larger resonance widths, signifying a lack of field confinement. Sensitivity was improved with a thickness of 1.5 nm, but R_{min} and resonance width were still not optimal. The optimal results were obtained at a thickness of 2 nm, where high sensitivities (541.42, 378.19, and 326.48 deg/RIU), low R_{min} values (0.011, 0.073, and 0.096), and relatively narrower FWHM (1.98, 1.5, and 1.32 deg) were achieved, resulting in better QF and FOM. Although a slight increase in sensitivity was noticed at 2.5 nm for the ring stage, higher reflectance and lower quality factors hampered the performance. A thickness of 3 nm resulted in marked deterioration, including a broadened resonance and lower sensitivity, owing to reduced penetration of the evanescent field and improper momentum matching. Hence, an HfO_2 layer thickness of 2 nm is chosen as the optimal design, providing high sensitivity, sharp resonance curves, and robust multi-stage malaria detection.

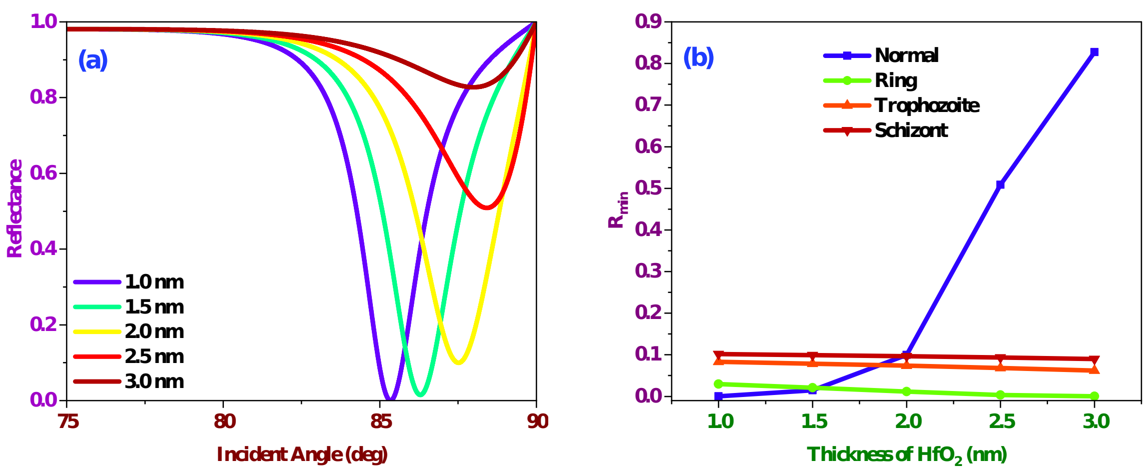

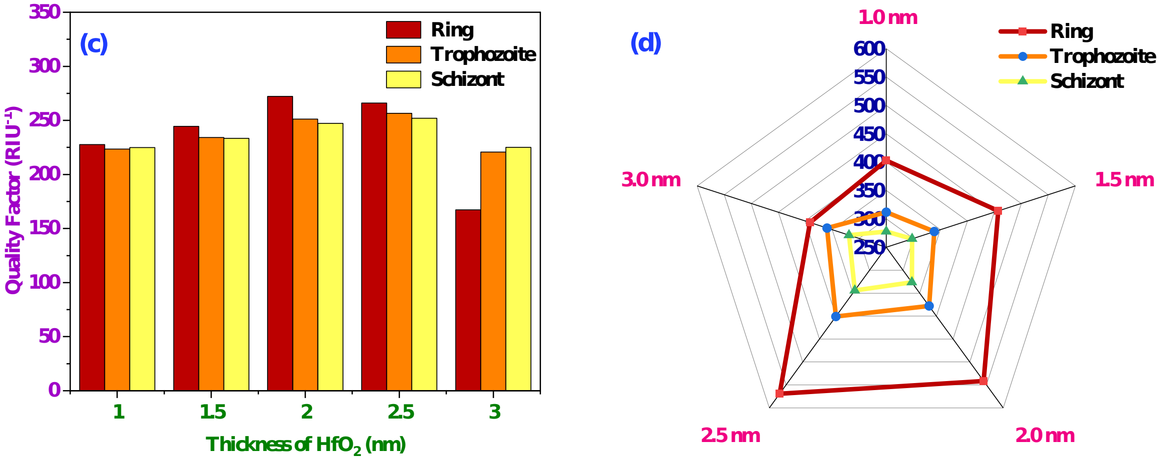

Fig. 8 Thickness variation of dielectric layer: (a) Reflectance vs Incident angle (Normal Stage), (b) R_{min}, (c) QF, and (d) Sensitivity.

3.6 Choosing 2D material

A comprehensive comparative analysis of various 2D materials used in the outer sensing layer of the biosensor clearly reveals the superiority of BP in terms of performance in the proposed SPR biosensor shown in Fig. 9. When BP is used, the sensor has a very high sensitivity of 541.43 deg/RIU with a sharp resonance width of 1.98 deg, a high DA of 0.502 deg^{-1}, and a FOM of over 269.08, which is a clear measure of superior resonance characteristics and sensing accuracy for ring stage. However, for other 2D materials used, the performance is clearly inferior. For MoS_2, the sensors have lower values of sensitivity of around 258, 308.57, and 285 deg/RIU, with broadened resonance widths of over 4.72, 3.175, and 2.67 deg, and much lower FOM values of 37.84, 86.25, and 98.01 for ring, trophozoite, and schizont stage, respectively, which is an indication of poor evanescent field enhancement. For WS_2, the sensors have lower values of sensitivity of 89.28, 289.57, and 276 deg/RIU, with broadened resonance widths of around 3.77, 2.3, and 1.94 deg, and much lower FOM values of 19.44, 125.28, and 141.52 for ring, trophozoite, and schizont stage, respectively, which is an indication of poor plasmon-analyte coupling. MXene has a moderate sensitivity of approximately 368 deg/RIU, but it has a wider resonance width of above 4.5 deg and a lower FOM of 56.60, which restricts the angular resolution. Likewise, graphene has yield sensitivity of 427.28, 325.95, and 288.41 deg/RIU, resonance widths of 2.5, 1.86, and 1.62 deg, and FOM of 166.31, 174.48, and 177.34 for ring, trophozoite, and schizont stage, respectively, thus reiterating its poorer sensing capability compared to BP. The better sensing capability of BP lies in its direct bandgap tunability, high in-plane anisotropy, and high carrier mobility, which together contribute to better confinement of electromagnetic fields and light-matter interaction at the sensing interface. As a result, BP supports steeper resonance curves, lower R_{min}, and much higher sensing resolution, thus explaining its choice over all other 2D materials for its high sensitivity, accuracy, and reliable malaria detection capabilities.

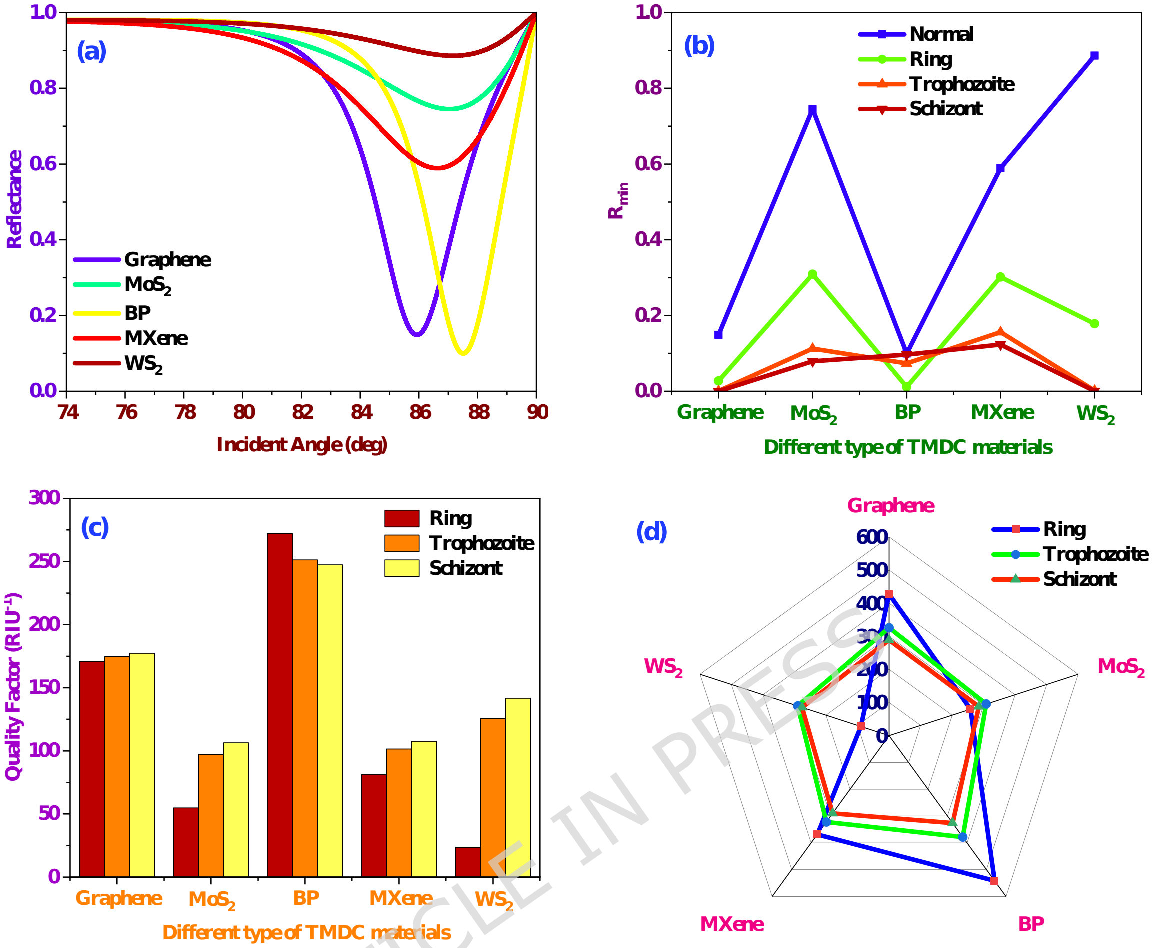

Fig. 9 Performance analysis using different TMDC materials: (a) Reflectance vs Incident angle (Normal Stage), (b) R_{min}, (c) QF, and (d) Sensitivity.

3.7 Layer Thickness Optimization of SPR Sensors via Brute-Force Search and Iterative Verification

Malaria continues to pose serious challenges in the domain of public health mainly owing to resistance to drugs in certain strains of Plasmodium and environmental factors contributing to its spreading. Detection at an early stage is of utmost importance, leading to the need for development of highly sensitive detectors. Among various methods employed in detecting malaria, SPR-based sensing devices are well known for their excellent sensitivity and fast responses. In the current study, a multilayer SPR sensor with the structure of N-FK51a+SiO_2+Cu+HfO_2+BP is utilized in detecting malaria. In order to have the optimal performance of the biosensor, an optimization approach is used to find the optimal thickness values of each layer of the multilayer structure. The approach ensures that we explore the global optimum solution rather than the local one. In this case, the thickness of BP remains constant whereas that of SiO_2 is changed within the range of 0 nm to 30 nm with an interval of 1 nm. On the other hand, the thickness of the Cu layer changes between 30 nm and 60 nm with an interval of 1 nm and that of HfO_2 varies within the range of 0 nm to 5 nm with an interval of 0.1 nm. This optimal combination is obtained at SiO_2 = 20 nm, Cu = 50 nm, and

HfO_2 = 2 nm, as the sensing element shows its best plasmonic behavior under this configuration. The transfer matrix method is used to analyze the reflectance spectrum of each layer combination in order to find out the critical parameters such as resonance angle, minimum reflectance, and resonance shift.

Before the regression analysis was carried out, Pearson correlation matrices were determined to examine the monotonicity between the input parameters and their corresponding output parameters, as shown in Fig. 10. Pearson correlation matrices provide a quantitative measure of the linear relationship between the input parameters and their corresponding output parameters. In this regard, the Pearson correlation coefficient r is used to assess the extent of correlation that exists between two parameters, x and y, where m observations are made. The mathematical representation of the Pearson correlation coefficient calculation is shown in the following equation [54]:

$$\frac{m\left(\sum xy\right) - \left(\sum x\right)\left(\sum y\right)}{\left[m\sum x^2 - \left(\sum x\right)^2\right] \times \left[m\sum y^2 - \left(\sum y\right)^2\right]} \quad (18)$$

The aim of linear regression analysis is to determine the line that most closely fits the relationship between the variables. It is also known as the regression line or line of greatest fit. It can be expressed by the equation below:

$$Y = \beta_0 + \beta_1 X_1 + \beta_2 X_2 + \ldots \beta_n X_n \quad (19)$$

Where Here, Y is the dependent (target) parameters, whereas X_1, X_2, …, X_n represent the independent (predictor) components. The symbol β_0 stands for the constant term, which is the value of the dependent variable when all the predictor variables are equal to zero. Similarly, β_1, β_2, …, β_n represent the regression weights that measure the importance of each independent variable on the dependent variable.

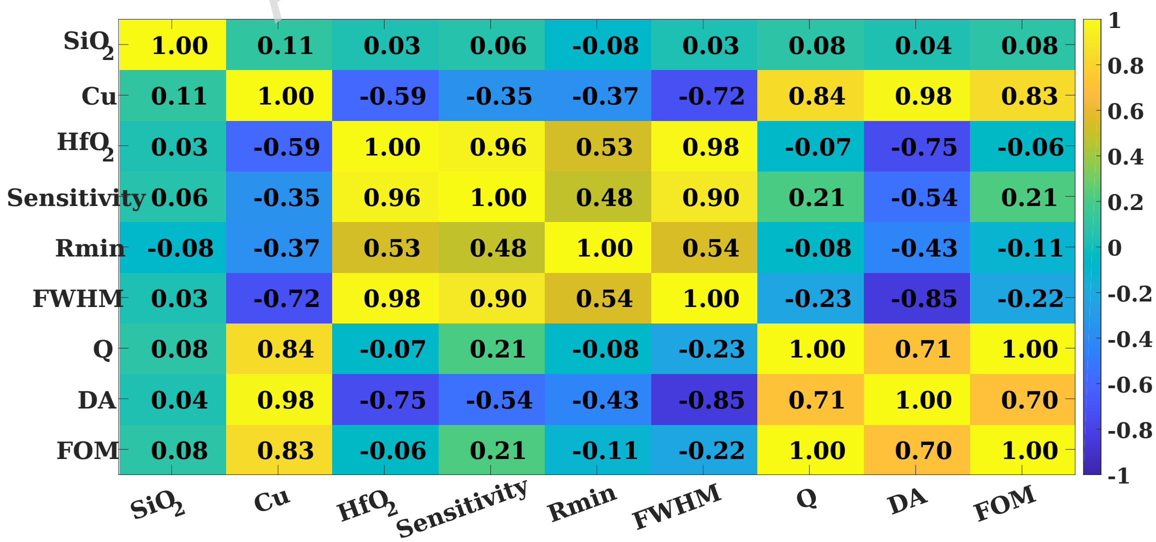

Fig. 10 Heat map showing correlations among design and performance metrics.

3.8 Performance Comparison of ANN, ANFIS and RBFNN Models for malaria detection Accuracy

To assess the prediction capability of the proposed SPR-based biosensor for malaria diagnosis, three advanced supervised intelligent modeling approaches, such as artificial neural network (ANN), adaptive neuro-fuzzy inference system (ANFIS), and radial basis function neural network (RBFNN), are used. These models are more appropriate for biosensing tasks due to their ability to handle complex nonlinear relationships among various SPR response variables and malaria stage changes. The FFBP-ANN model uses a multilayer feed-forward network trained with backpropagation to approximate the nonlinear input-output relationships. The ANFIS model combines neural learning with fuzzy rule-based systems, which are capable of efficiently dealing with the uncertainty and nonlinear variations involved in the SPR sensing data. The RBFNN model, on the other hand, uses localized radial basis activation functions, which provide faster convergence and better generalization properties for modeling highly nonlinear sensor responses. For all three models, the input variables are θ_{res}, R_{min}, and FWHM, and the output variable is the corresponding malaria stage. In terms of the ML approach, a total number of 1000 simulated samples were generated from the SPR sensor output responses at various refractive indices corresponding to the stages of malaria infection. Out of these samples, 1000 were used for training, and the remaining 300 were used for validation. The inputs for all the models were θ_{res}, R_{min}, and FWHM, whereas the output variable was the malaria infection stage classification.

For the ANN model, a feed-forward back propagation neural network with one hidden layer, which had ten neurons, was adopted. Training of the ANN model was done by adopting the Levenberg-Marquardt optimization technique. For the ANFIS model, a Sugeno-type fuzzy inference system, in which the membership functions were Gaussian, was used to capture the nonlinear relation between the sensor output responses and the different stages of malaria. An RBFNN model was built using radial basis neurons with the spread parameter optimized empirically for optimal convergence. Evaluation of the performance of all models was done using the prediction error and standard deviation of the prediction errors. The comparison between the actual values of the malaria stages and the predicted values by the FFBP-ANN, ANFIS, and RBFNN models is shown in Fig. 11(a), Fig. 11(c), and Fig. 11(e), respectively. The error curves for the predicted values of all three models are shown in Fig. 11(b), Fig. 11(d), and Fig. 11(f), respectively. The results are in good agreement with the target values for all models, and the learning of the sensor analyte relationship is successful. Error analysis provides information on the performance of all three models.

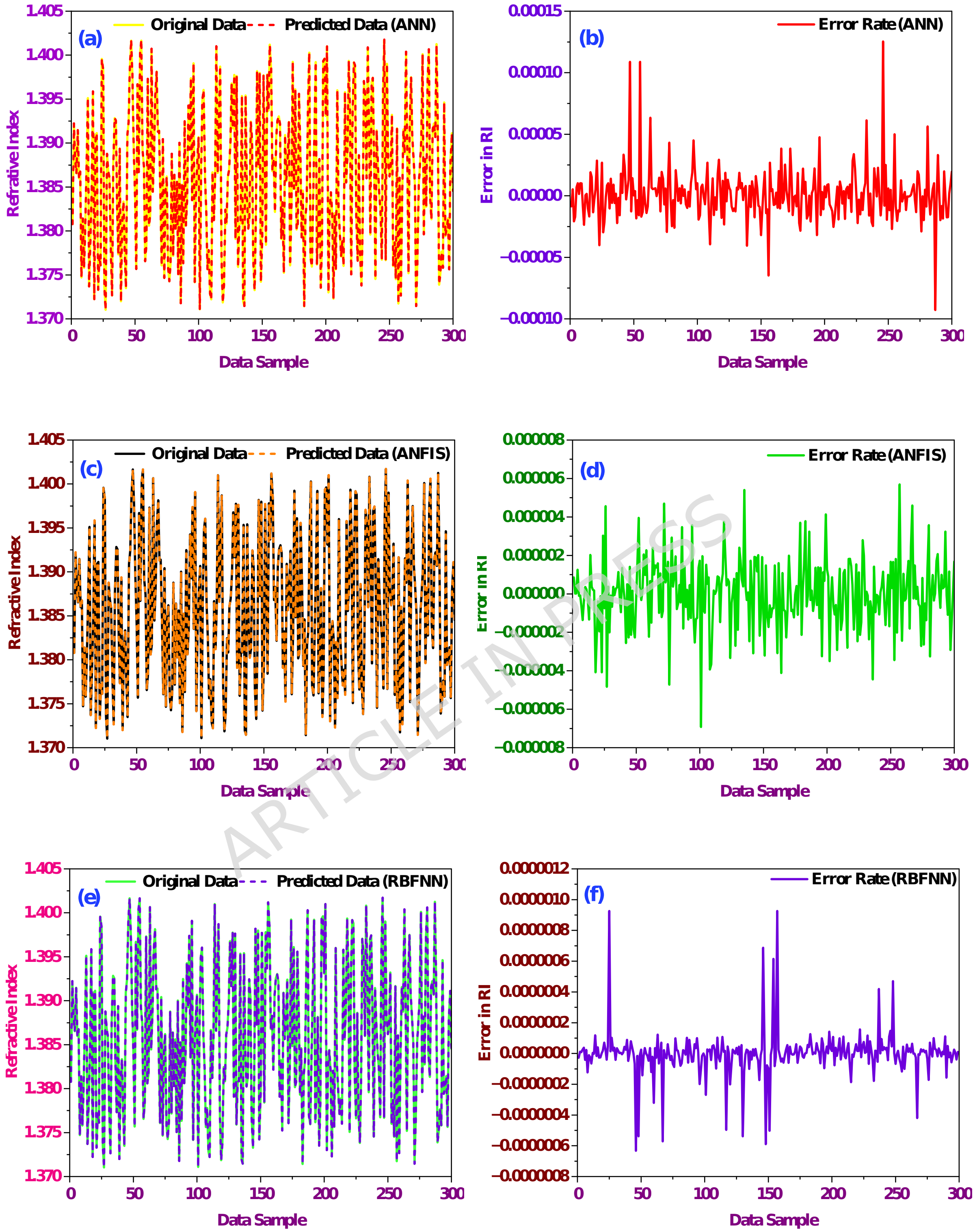

Fig. 11 Machine learning-based analysis for the evaluation of the accuracy of prediction for Malaria detection: (a) Original vs ANN-predicted data, (b) Error analysis for ANN models, (c) Original vs ANFIS-predicted data, (d) Error analysis for the

proposed models, (e) Original vs RBFNN-predicted data, and (f) Error analysis for RBFNN models.

The ANN has a maximum prediction error of about 2.82×10^{-4} with a standard deviation of around 0.0780. The ANFIS shows better accuracy, with a lower maximum error of about 7.65×10^{-6} and a standard deviation of 0.0059. It is important to note that the RBFNN model has the lowest prediction error, with a maximum error of close to 9.83×10^{-7} and a standard deviation of 0.0004, which clearly shows better accuracy and stability. The better performance of RBFNN is due to its localized learning ability and effective modeling of the nonlinear variations in the SPR response data. In conclusion, although all three intelligent models show strong predictive capability, RBFNN clearly outperforms both FFBP-ANN and ANFIS in terms of accuracy, stability, and error minimization, thus proving its effectiveness for precise malaria stage identification with the proposed SPR biosensing platform. The decision curve based on RI, as described as a systematic stage identification tool for malaria diagnosis, linking optical RI values with the severity of infection. Every stage of malaria has a unique RI value of red blood cells, which depends on the stage of infection: normal (1.402), ring (1.395), trophozoite (1.381), and schizont (1.371). To account for the physiological differences and uncertainties in measurement, a tolerance interval of ±10% is considered around each reference value. The RI values that lie in these marked areas show a prominent dominance of the respective infection stages, while values outside these areas indicate a transition from one stage to another. As shown in Fig. 12, this systematic mapping enables the conversion of continuous optical values into meaningful stage labels. The decision curve also helps to maintain consistency between the SPR sensor's optical signal and the stage identification results provided by the FFBP-ANN and ANFIS models.

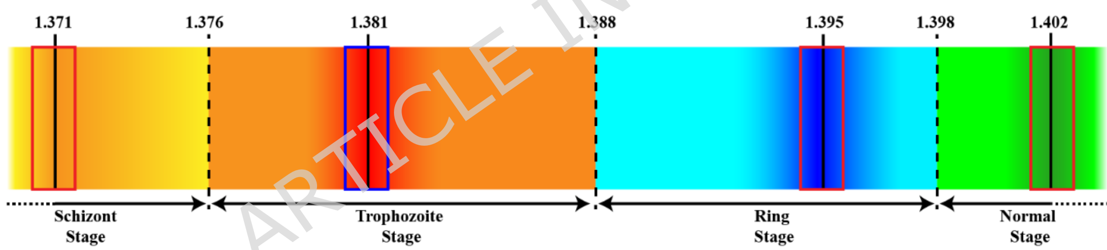

Fig.12 Refractive index-based malaria stage decision curve.

3.9 Fabrication Tolerance and Feasibility Analysis

To properly assess the fabrication feasibility of the proposed SPR biosensor, a comprehensive fabrication tolerance analysis was conducted by introducing systematic variations of ±10% in the thickness of the metallic and dielectric layers. The thickness of the BP layer was intentionally fixed due to its dominant role in the electromagnetic field confinement and overall biosensing performance. In the initial stage, the biosensor sensitivity to individual fabrication tolerances was investigated by introducing independent variations of ±10% in the thickness of the SiO_2, Cu, and HfO_2 layers, while fixing all other variables to their optimized settings. The corresponding changes in the reflectance responses and associated performance parameters are shown in ~~Fig. 12~~ Fig. 13. Subsequently, a full combined tolerance analysis was carried out by simultaneously varying the thicknesses of all three layers (SiO_2/Cu/HfO_2) by ±10%, thus accurately simulating real-world inaccuracies introduced during fabrication. The variation in key performance parameters is summarized in Table 4. It is evident from the analysis that both individual and combined thickness variations result in negligible performance degradation, thus establishing the robustness of the proposed biosensor against fabrication inaccuracies. These results unequivocally establish the experimental feasibility of the biosensor and establish that it can be fabricated using standard thin-film deposition techniques.

Table 4. Influence of ±10% thickness error on the performance parameters of the proposed sensor (Ring Stage)

Performance parameter	**Error possibility of all layers for +10%**	**Error possibility of all layers for -10%**
Sensitivity (deg/RIU)	577.5714	438.2857
R_{min}	0.0301	0.1394
FWHM	1.7530	2.4060
DA (deg^{-1})	0.5705	0.4156
QF (RIU^{-1})	329.4760	182.1636
FOM	319.5567	156.7690

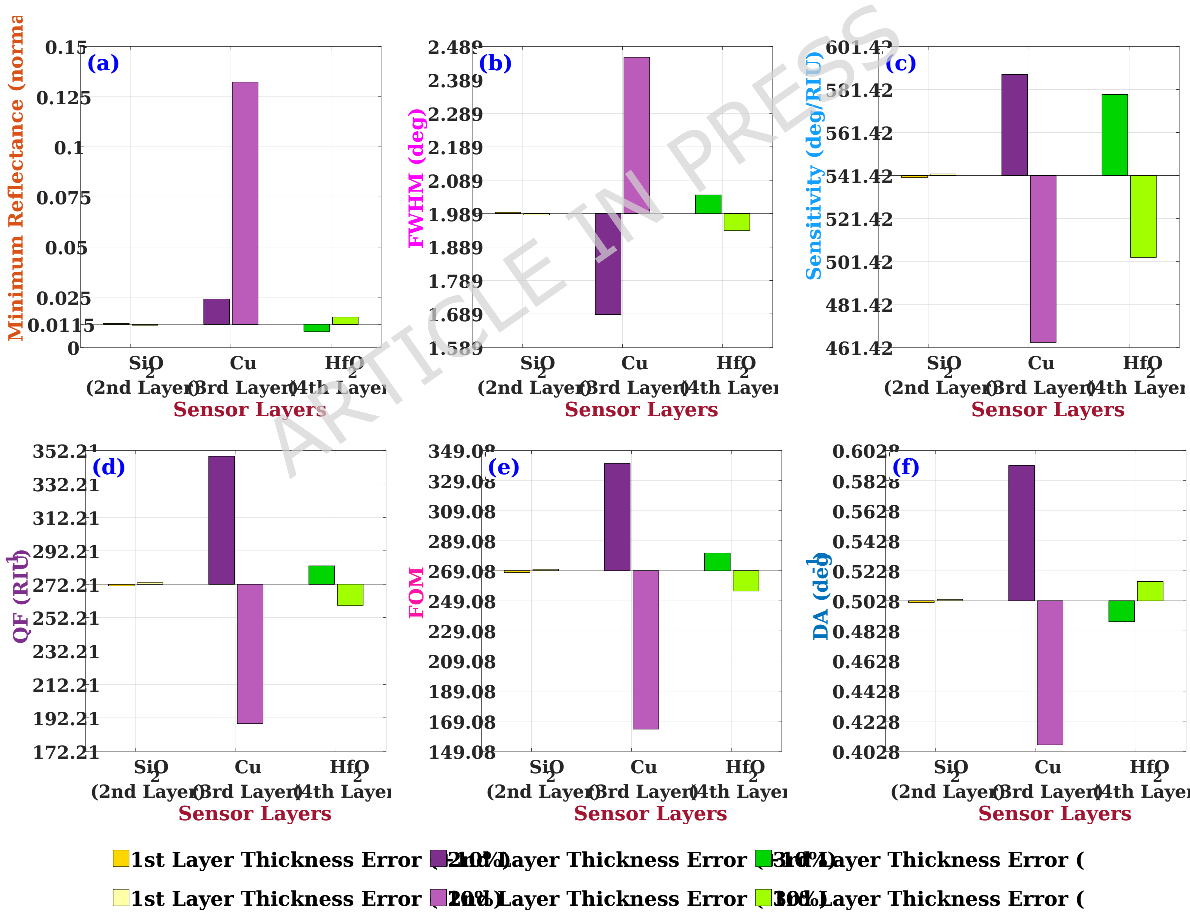

Fig. 13 Fabrication Tolerance Analysis of the Proposed SPR Biosensor under ±10% Layer Thickness Variation and showing performance metrics (a) R_{min}, (b) FWHM, (c) Sensitivity, (d) QF, (e) FOM, and (f) DA.

3.10 Electric field analysis and penetration depth

The surface plasmon resonance excited with high intensity in the proposed sensor design is validated based on the electric field intensity distribution calculated at an analyte refractive index of 1.402 and a resonance angle of 87.51 deg, as shown in Fig. 14. The field extends into the sensing medium, decaying exponentially from its peak value at the sensor-analyte interface. For the optimized design, the penetration depth (PD) is calculated to be about 208 nm. This result is obtained using both the FEM and FDTD methods, showing a strong consistency between the two simulation methods and hence validating the accuracy of the simulation results. The penetration depth is the distance from the interface where the electric field intensity drops to 1/e (about 37%) of its peak value at the sensor-analyte interface value [55]. The presence of strong near-surface field confinement and a relatively large penetration depth increase the effective interaction volume between the evanescent field and the analyte. As a result, the excited surface plasmon wave is highly sensitive to RI changes in the sensing region, resulting in enhanced detection capability and overall sensing performance. All the performance parameter of the proposed SPR biosensor is given in Table 5.

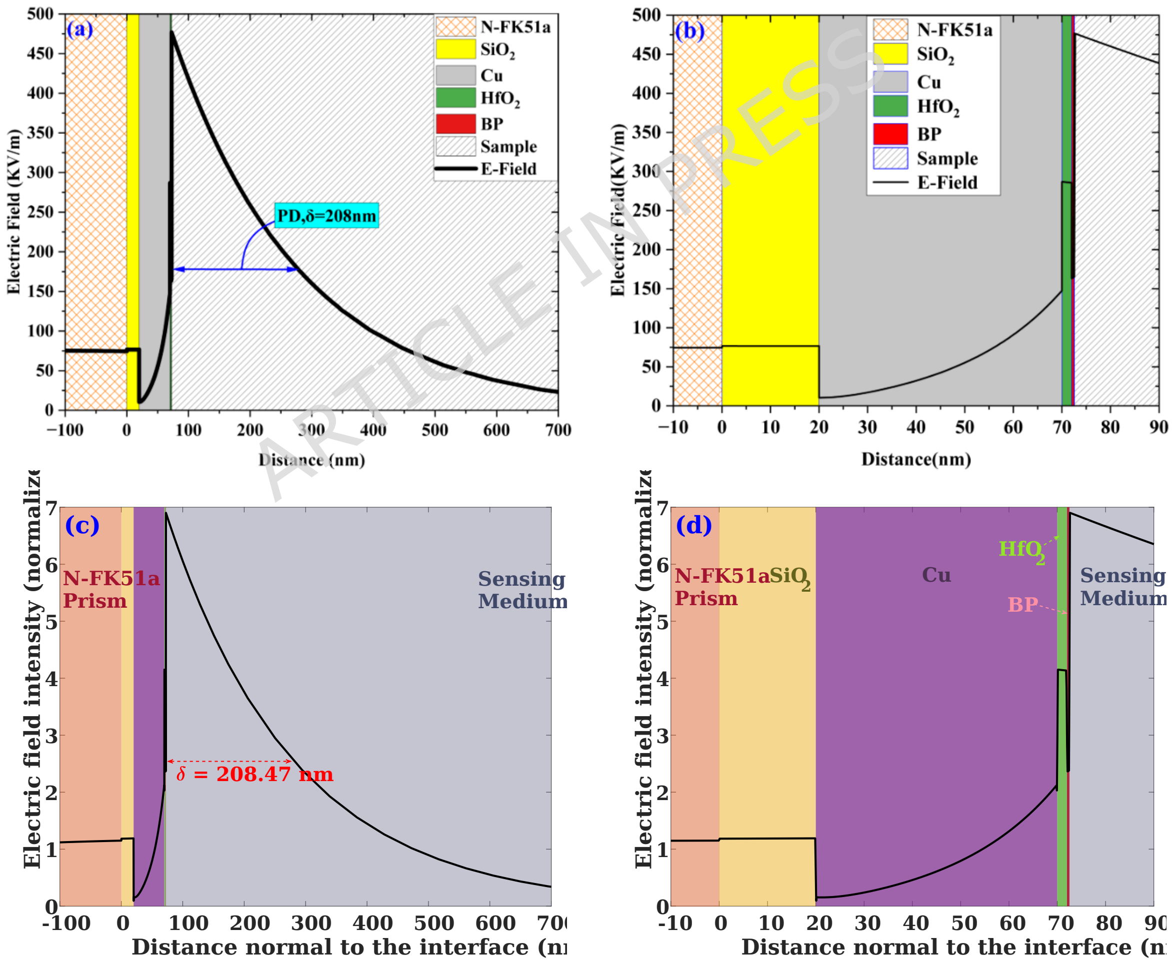

Fig. 14 (a) Penetration depth using FEM method, (b) Electric field intensity to the normalized distance for the proposed sensor using FEM method, (c) Penetration depth using FDTD method, and (d) Electric field intensity to the normalized distance for the proposed sensor using FDTD method.

Table 5. Performance enhancement metrics across all malaria stages

Malaria stage	RI	FWHM (deg)	R_{min}	θ_{res} (deg)	QF (RIU^{-1})	Sensitivity (deg/RIU)	DA (deg^{-1})	FOM
Normal	1.402	2.940	0.099	87.51	-	-	-	-
Ring	1.395	1.989	0.011	83.72	272.21	541.42	0.502	269.08
Trophozoite	1.381	1.505	0.073	79.57	251.28	378.19	0.664	232.76
Schizont	1.371	1.320	0.096	77.39	247.33	326.48	0.757	223.46

3.11 Wide Dynamic Range and Linearity of the Proposed SPR Biosensor

The correlation between the RI of malaria analytes and the resonance angle of the proposed SPR sensor is demonstrated in Fig. 15(a) using linear and polynomial curve fitting techniques. The RI of the analyte ranges from 1.371 to 1.402, resulting in a variation of the resonance angle from 76 deg to 88 deg. The linear relationship between the resonance angle and the RI is expressed by the equation □=−337.36022+302.04163□, while the polynomial behavior is represented by □=10649.70719−15553.0182□+5719.71855□^{2}. The values of the coefficients of determination for both curve fittings are R^2 = 0.97606 for the linear relationship and R^2 = 0.99645 for the polynomial relationship. The close-to-unity values of R2 indicate that the proposed SPR sensor has a perfectly linear relationship within the measured RI range. Fig. 15(b) also shows the reflectance as a function of incident angle for different RIs representing various stages of malaria. A systematic shift of the resonance dip towards higher angles with increasing RI values, along with distinct minima, is observed. This indicates the high precision, stability, and reliability of the proposed biosensor, thus confirming its suitability for precise malaria detection based on its predictable RI sensitivity.

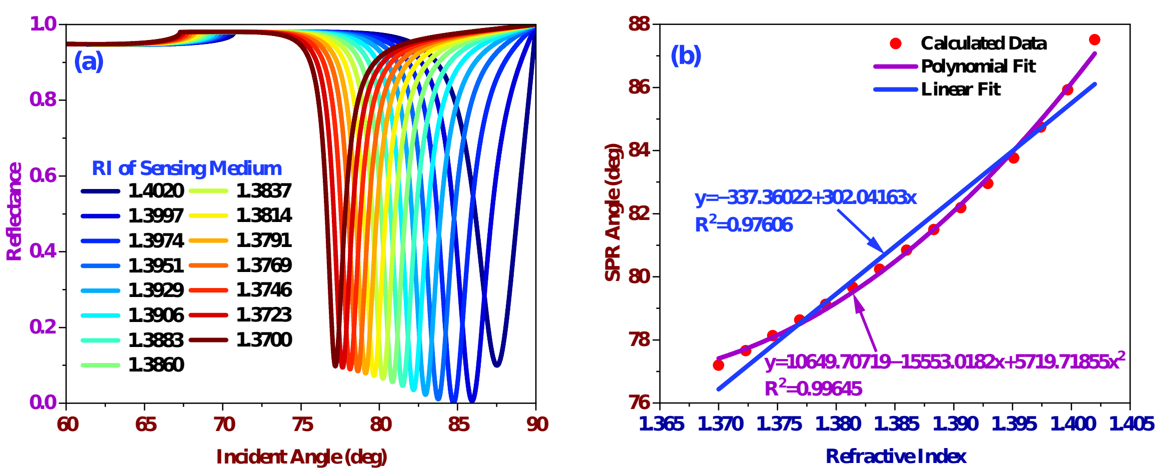

Fig. 15 (a) Reflectance vs Incident angle (deg) for RI 1.3700 to 1.4020, and (b) The RI of the corresponding malaria is polynomial and linear correlated with the resonance dip angle.

Table 6. Performance Comparison of the Proposed SPR Sensor with Previously Reported SPR Sensors

Malaria stages	Ref work	Sensor Configuration	Sensitivity (deg/RIU)	DA (deg^{-1})	QF (RIU^{-1})	Year
Ring stage	Proposed work	N-FK51a+SiO_2+Cu+HfO_2+BP	541.42	0.502	272.21	-
	Ref work-1 [56]	BK7+TiO_2+Ag+Si+BP	494.57	0.378	187.34	2025
	Ref work-2 [57]	Ag+Si_3N_4+BP/ssDNA (Sys_4)	464.38	0.873	124.81	2025
	Ref work-3 [18]	BK7+ZnTe+Ag+Fe_2O_3 + BlueP/WS_2	444.00	0.215	95.83	2025
	Ref work-4 [58]	BK7+Cu+TiO_2+TeO_2+BP	432.83	0.509	220.71	2025
	Ref work-5 [59]	BK7+Ag+ZnTe+Fe_2O_3+BP	370.00	0.454	168.02	2025
	Ref work-6 [60]	BK7+Ag+Si_3N_4+Graphene+ssDNA	353.14	0.507	72.49	2025
Trophozoite stage	Proposed work	N-FK51a+SiO_2+Cu+HfO_2+BP	378.19	0.664	251.28	2025
	Ref work-1 [56]	BK7+TiO_2+Ag+Si+BP	371.33	0.536	199.32	2025
	Ref work-2 [57]	Ag+Si_3N_4+BP/ssDNA (Sys_4)	343.93	0.873	124.81	2025
	Ref work-3 [18]	BK7+ZnTe+Ag+Fe_2O_3+ BlueP/WS_2	341.04	0.261	89.18	2025
	Ref work-4 [58]	BK7+Cu+TiO_2+TeO_2+BP	328.11	0.683	224.27	2025
	Ref work-5 [59]	BK7+Ag+ZnTe+Fe_2O_3+BP	300.00	0.609	182.70	2025
	Ref work-6 [60]	BK7+Ag+Si_3N_4+Graphene+ssDNA	291.14	1.447	68.90	2025

Schizont stage	Proposed work	N-FK51a+SiO_2+Cu+ HfO_2+BP	326.48	0.757	247.33	2025
	Ref [56] work-1	BK7+TiO_2+Ag+Si + BP	324.26	0.619	200.78	2025
	Ref [57] work-2	Ag+Si_3N_4+BP/ssDNA (Sys_4)	301.07	3.043	98.17	2025
	Ref [18] work-3	BK7+ZnTe+Ag+Fe_2O_3 + BlueP/WS_2	300.74	0.283	85.36	2025
	Ref [58] work-4	BK7+Cu+TiO_2+TeO_2 +BP	290.56	0.783	227.71	2025
	Ref [59] work-5	BK7+Ag+ZnTe+ Fe_2O_3+BP	270.00	0.788	207.37	2025
	Ref [60] work-6	BK7+Ag+Si_3N_4+ Graphene+ssDNA	263.25	2.091	67.46	2025

The performance of the proposed sensor is systematically compared with six recently reported structures across different malaria infection stages in terms of sensitivity and QF as mentioned in Table 6. For the ring stage, the proposed sensor exhibits a notable enhancement in sensitivity, showing improvements of approximately 9.47%, 16.59%, 21.94%, 25.09%, 46.33%, and 53.32% compared to ref-1 through ref-6, respectively, along with a remarkable improvement in QF of about 45.30%, 118.10%, 184.06%, 23.33%, 62.01%, and 275.51%. Similarly, during the trophozoite stage, the proposed design demonstrates consistent sensitivity enhancement of approximately 1.85%, 9.96%, 10.90%, 15.27%, 26.06%, and 29.92% over ref-1 to ref-6, respectively, while the QF is significantly increased by about 26.04%, 101.16%, 181.86%, 12.05%, 37.54%, and 264.72%. Furthermore, for the schizont stage, sensitivity improvements of approximately 0.69%, 8.44%, 8.56%, 12.36%, 20.92%, and 24.02% are achieved compared to the corresponding ref works, accompanied by substantial QF enhancements of about 23.18%, 151.90%, 189.80%, 8.61%, 19.27%, and 266.60%. The consistently higher sensitivity and significantly improved QF for all stages of malaria confirm sharper resonance characteristics, better signal resolution, and robust RI sensing performance, thus validating the efficacy and reliability of the proposed sensor for precise multi-stage malaria detection.

Conclusion

The proposed work presents a highly optimized multilayer surface plasmon resonance (SPR) biosensor for the sensitive and reliable detection of malaria at three clinically significant stages of infection. By using a N-FK51a+SiO_2+Cu+HfO_2+BP layer architecture, the proposed biosensor shows outstanding performance, with a maximum angular sensitivity of 541.42 deg/RIU, a sharp resonance linewidth with FWHM of 1.98 deg, a DA of 0.502 deg^{-1}, and a high QF of 272.21 RIU^{-1} for ring stage, ensuring accurate and reliable measurements. The outstanding sensing performance is achieved by the combined effect of the multilayer architecture, where the SiO_2 and Cu layers provide efficient plasmon excitation and optical confinement, the HfO_2 layer provides improved structural stability and biocompatibility, and the BP sensing layer provides substantial enhancement of the evanescent electric field and improved analyte-surface interactions. The proposed biosensor shows high efficacy in detecting the most important malaria biomarkers, such as Plasmodium lactate dehydrogenase (pLDH), which is a biomarker of active parasitic metabolism and allows infection stage-specific monitoring, and histidine-rich protein-2 (HRP-2), which is a highly specific and widely accepted biomarker for rapid malaria diagnosis. The prediction of sensor response is further verified using three supervised intelligent models, namely feed-forward backpropagation ANN, ANFIS, and RBFNN. Although all models demonstrate strong learning and generalization performance, RBFNN outperforms the others in terms of prediction accuracy with lower error due to its adaptive rule-based inference system, which is highly beneficial for modeling a nonlinear SPR sensor response. The high sensitivity of the proposed sensor to refractive index changes related to these biomarkers clearly indicates the clinical significance of the proposed sensor for early and accurate malaria detection. In addition, the high linearity of the sensor response clearly confirms the robustness of the proposed sensor for real-time diagnostics. Due to its improved sensitivity, stability, and scalability, the proposed SPR biosensor also has strong potential for implementation in other infectious and chronic disease detection platforms.

Funding

This research did not receive any specific grant from funding agencies in the public, commercial, or not-for-profit sectors.

Data availability

All data generated or analyzed during this study are included in this published article.

References

1. Tangpukdee, N., Duangdee, C., Wilairatana, P. & Krudsood, S. Malaria diagnosis: A brief review. *Korean Journal of Parasitology* vol. 47 93–102 Preprint at https://doi.org/10.3347/kjp.2009.47.2.93 (2009).

2. Ramos-Briceño, D. A., Flammia-D'Aleo, A., Fernández-López, G., Carrión-Nessi, F. S. & Forero-Peña, D. A. Deep learning-based malaria parasite detection: convolutional neural networks model for accurate species identification of Plasmodium falciparum and Plasmodium vivax. *Sci. Rep.* **15**, 3746 (2025).

3. Obeagu, E. I., UO, C. & IS, E. Malaria Rapid Diagnostic Test (RDTs). *Ann. Clin. Lab. Res.* **06**, (2018).

4. Kumar, P., Kumar, R., Singh, M. K. & Ahmed, B. Detection of Plasma, Platelets, Hemoglobin in Blood Sample of Dengue Malaria Based on Surface Plasmon Resonance Biosensor Using Black Phosphorus: A Numerical Analysis. *Plasmonics* **19**, 1779–1790 (2024).

5. Singh, S. *et al.* Theoretical Study of Malaria Detection in Blood Samples Using Bimetal Layer and Zinc Telluride Nanomaterial-Based Surface Plasmon Resonance Biosensor. *Plasmonics* **18**, 2125–2136 (2023).

6. Uniyal, A. *et al.* A Novel SPR Sensor Response for Chemical Sensing of Organic Solvents: A Computational Approach. *Adv. Theory Simul.* **9**, e02113 (2026).

7. Jana, J., Ganguly, M. & Pal, T. Enlightening surface plasmon resonance effect of metal nanoparticles for practical spectroscopic application. *RSC Adv.* **6**, 86174–86211 (2016).

8. Uniyal, A., Pal, A. & Chauhan, B. Long-range SPR sensor employing platinum diselenide and cytop nanolayers giving improved performance. *Physica B Condens. Matter* **649**, 414487 (2023).

9. Shivangani *et al.* Numerical Study to Enhance the Sensitivity of a Surface Plasmon Resonance Sensor with BlueP/WS2-Covered Al2 O3-Nickel Nanofilms. *Nanomaterials* **12**, (2022).

10. Srivastava, S., Singh, S., Mishra, A. C., Lohia, P. & Dwivedi, D. K. Numerical Study of Titanium Dioxide and MXene Nanomaterial-Based Surface Plasmon Resonance Biosensor for Virus SARS-CoV-2 Detection. *Plasmonics* **18**, 1477–1488 (2023).

11. Karki, B., Uniyal, A., Srivastava, G. & Pal, A. Black Phosphorous and Cytop Nanofilm-Based Long-Range SPR Sensor with Enhanced Quality Factor. *J. Sens.* **2023**, (2023).

12. Singh, S. *et al.* Theoretical study of perovskite nano material based surface plasmon resonance biosensor for cancers cell detection. *Optik (Stuttg).* **289**, 171259 (2023).

13. Pal, A. *et al.* Surface plasmon resonance sensor for dopamine detection based on CeO2 nanorod and ZnO nanosheet. *Journal of Materials Science: Materials in Electronics* **37**, (2026).

14. Srivastava, T., Jha, R. & Das, R. High-performance bimetallic SPR sensor based on periodic-multilayer-waveguides. *IEEE Photonics Technology Letters* **23**, 1448–1450 (2011).

15. Srivastava, A., Verma, A., Das, R. & Prajapati, Y. K. A theoretical approach to improve the performance of SPR biosensor using MXene and black phosphorus. *Optik (Stuttg).* **203**, 163430 (2020).

16. Singh, Y. *et al.* Highly Sensitive Plasmonic Biosensor for the Detection of Chikungunya Virus Employing TiO2 and BP/WS2 Heterostructure. *Plasmonics* https://doi.org/10.1007/s11468-024-02242-3 (2024) doi:10.1007/s11468-024-02242-3.

17. Krampa, F. D., Aniweh, Y., Kanyong, P. & Awandare, G. A. Recent advances in the development of biosensors for malaria diagnosis. *Sensors (Switzerland)* vol. 20 Preprint at https://doi.org/10.3390/s20030799 (2020).

18. Utshob, Md. A. A. I. *et al.* Design of a highly sensitive SPR biosensor for rapid malaria detection based on zinc telluride and blue phosphorus/tungsten disulfide material. *Biosens. Bioelectron. X* **27**, 100709 (2025).

19. Rafi, S. A. *et al.* Optical Based Surface Plasmon Resonance Sensor for the Detection of the Various Kind of Cancerous Cell. *Cell Biochem. Biophys.* **83**, 689–715 (2025).

20. Bouandas, H., Kumar, R., Singh, S., Bouazzi, Y. & Sirohi, K. Enhanced sensitivity and figure of merit in surface plasmon resonance biosensors with silicon dioxide and barium titanate materials. *Microchemical Journal* **212**, 113341 (2025).

21. Alagu Vibisha, G. *et al.* Designing high sensitivity and high figure of merit SPR biosensor using copper and 2D material on CaF2 prism. *Results in Optics* **11**, (2023).

22. Tiwari, K., Sharma, S. C. & Hozhabri, N. Hafnium dioxide as a dielectric for highly-sensitive waveguide-coupled surface plasmon resonance sensors. *AIP Adv.* **6**, (2016).

23. Khan, Md. B., Hossain, B., Rahman, T., Ahmed, D. M. S. & Paul, A. K. Design and Analysis of a Highly Sensitive BaTiO3—BP Hybrid Structure-Based SPR Biosensor for Rapid Bacterial Detection. *Plasmonics* https://doi.org/10.1007/s11468-025-02798-8 (2025) doi:10.1007/s11468-025-02798-8.

24. Kumar, A., Kumar, A. & Srivastava, S. K. Silicon Nitride-BP-Based Surface Plasmon Resonance Highly Sensitive Biosensor for Virus SARS-CoV-2 Detection. *Plasmonics* **17**, 1065–1077 (2022).

25. Inthiyaz, S. *et al.* Skin disease detection using deep learning. *Advances in Engineering Software* **175**, 103361 (2023).

26. Wekalao, J., Mandela, N., Mwendwa, G., Elamri, O. & Maamar, A. E. T. Advanced plasmonic sensor design for sperm detection with machine learning-driven optimization. *Opt. Quantum Electron.* **57**, (2025).

27. Ansari, G., Pal, A., Srivastava, A. K. & Verma, G. Machine learning approach to surface plasmon resonance bio-chemical sensor based on nanocarbon allotropes for formalin detection in water. *Sens. Biosensing Res.* **42**, 100605 (2023).

28. Jiang, J., Chen, M. & Fan, J. A. Deep neural networks for the evaluation and design of photonic devices. *Nature Reviews Materials* vol. 6 679–700 Preprint at https://doi.org/10.1038/s41578-020-00260-1 (2021).

29. Spall, J., Guo, X. & Lvovsky, A. I. Training neural networks with end-to-end optical backpropagation. *Advanced Photonics* **7**, (2025).

30. Panda, A. & Pukhrambam, P. D. Modeling of High-Performance SPR Refractive Index Sensor Employing Novel 2D Materials for Detection of Malaria Pathogens. *IEEE Trans. Nanobioscience* **21**, 312–319 (2022).

31. Agnero, M. A. *et al.* Malaria-infected red blood cell analysis through optical and biochemical parameters using the transport of intensity equation and the microscope's optical properties. *Sensors (Switzerland)* **19**, (2019).

32. Juwel, M. B. *et al.* Design and optimization of a hybrid SPR biosensor for highly sensitive detection of carcinoembryonic antigen. *Next Materials* **10**, (2026).

33. Juwel, M. B. *et al.* Niobium pentoxide and black phosphorus based multilayer surface plasmon resonance biosensor for the detection of ultra-sensitive mycobacterium tuberculosis. *J. Comput. Electron.* **25**, 55 (2026).

34. Marcos, L. V. R., Larruquert, J. I., Méndez, J. A. & Aznárez, J. A. Self-consistent optical constants of SiO2 and Ta2O5 films. *Opt. Mater. Express* **6**, 3622–3637 (2016).

35. Singh, N. P. *et al.* Numerical analysis of silicon nitride and perovskite nanomaterial assisted SPR biosensor for dengue cell detection. *Journal of Optics (India)* https://doi.org/10.1007/s12596-024-02224-y (2024) doi:10.1007/s12596-024-02224-y.

36. Pandey, P. S., Kumar Raghuwanshi, S., Singh, R. & Kumar, S. magnetochemistry Surface Plasmon Resonance Biosensor Chip for Human Blood Groups Identification Assisted with Silver-Chromium-Hafnium Oxide. https://doi.org/10.3390/magnetochemistry (2023) doi:10.3390/magnetochemistry.

37. Vasimalla, Y., Kaur, B. & Kumar, S. Metallic Layer-Based SPR Biosensor for Mycobacterium Tuberculosis Detection Employing Zinc Oxide and TMDCs Heterostructure. *IEEE Transactions on Plasma Science* **52**, 5350–5357 (2024).

38. Mousania, Y., Karimi, S. & Farmani, A. Designing High-Performance SPR Biosensor Using Hybrid Structure of BifeO3 and 2D Material for SARS-CoV-2 Detection. *Plasmonics* **20**, 7209–7228 (2025).

39. Lertvachirapaiboon, C., Baba, A., Shinbo, K. & Kato, K. Dual-mode surface plasmon resonance sensor chip using a grating 3D-printed prism. *Anal. Chim. Acta* **1147**, 23–29 (2021).

40. Ghodrati, M., Mir, A. & Farmani, A. Numerical analysis of a surface plasmon resonance based biosensor using molybdenum disulfide, molybdenum trioxide, and MXene for the diagnosis of diabetes. *Diam. Relat. Mater.* **132**, 109633 (2023).

41. Dakhlaoui, H. & Belhadj, W. Optimization of biosensor based on nitride-photonic crystal operating in visible range for Glucose detection. *Results in Engineering* **26**, 105430 (2025).

42. Uniyal, A. *et al.* Fluorinated graphene and CNT-based surface plasmon resonance sensor for detecting the viral particles of SARS-CoV-2. *Physica B Condens. Matter* **669**, 415282 (2023).

43. Akib, T. B. A. *et al.* Design and numerical analysis of a graphene-coated spr biosensor for rapid detection of the novel coronavirus. *Sensors* **21**, (2021).

44. Karki, B., Uniyal, A., Sarkar, P., Pal, A. & Yadav, R. B. Sensitivity Improvement of Surface Plasmon Resonance Sensor for Glucose Detection in Urine Samples Using Heterogeneous Layers: An Analytical Perspective. *Journal of Optics (India)* **53**, 2567–2577 (2024).

45. Almawgani, A. H. M. *et al.* Sensitivity enhancement of optical plasmon-based sensor for detection of the hemoglobin and glucose: a numerical approach. *Opt. Quantum Electron.* **55**, (2023).

46. Maurya, P., Kushwaha, A. & Verma, R. High Performance SPR Gas Sensor by Using Heterostructure of 2D Materials Graphene / Black Phosphorous / MoS 2. *Sens. Imaging* 1–20 (2024) doi:10.1007/s11220-024-00518-w.

47. Utshob, Md. A. A. I., Juwel, M. B., Rahman, M. M. A., Imam, S.-A. & Ishtiak, K. M. Integration of computational optics and machine learning for optimized SPR-based carcinoembryonic antigen detection. *Biomed. Opt. Express* **17**, 1825 (2026).

48. Ishtiak, K. M., Imam, S. Al & Khosru, Q. D. M. Graphene-Based Surface Plasmon Resonance Sensor for Water Salinity Concentration Detection Using Multiple Light Source Techniques. *IEEE Access* **11**, 130601–130617 (2023).

49. Kumar, U. A., Alqahtani, A. S., Mubarakali, A., Parthasarathy, P. & Uniyal, A. Transfer matrix modelling of a GdF3/MoS2 enhanced SPR sensor for label-free quantitative urine glucose detection in diabetes management: a simulation-based study. *J. Comput. Electron.* **25**, (2026).

50. Rafsan, A. A. *et al.* Surface plasmon resonance–based biosensor for accurate and rapid detection of Mycobacterium tuberculosis. *Microchimica Acta* **192**, (2025).

51. Bouandas, H., Kumar, R., Benhaliliba, M., Singh, S. & Garia, L. Plasmonic sensor design: Cu-SiO_2-Ni-black phosphorus for enhanced surface plasmon resonance in visible regime. *Microchimica Acta* **192**, (2025).

52. Kukli, K. *et al. Atomic Layer Deposition of HfO 2 Thin ®lms and Nanolayered HfO 2 ±Al 2 O 3 ±Nb 2 O 5 Dielectrics*.

53. Liu, X. *et al.* Black Phosphorus Based Field Effect Transistors with Simultaneously Achieved Near Ideal Subthreshold Swing and High Hole Mobility at Room Temperature. *Sci. Rep.* **6**, (2016).

54. Nurrohman, D. T. & Chiu, N.-F. Surface Plasmon Resonance Biosensor Performance Analysis on 2D Material Based on Graphene and Transition Metal Dichalcogenides. *ECS Journal of Solid State Science and Technology* **9**, 115023 (2020).

55. Emon, W. *et al.* Highly sensitive ZnO/Ag/BaTiO3/MoS2 hybrid structure-based surface plasmon biosensor for the detection of mycobacterium tuberculosis bacteria. *Optics Continuum* **3**, 495–512 (2024).

56. Kumar Roy, K. *et al.* Pioneering Malaria Diagnostics with a Multi-layered BK7/TiO2/Ag/Si/BP SPR Biosensor: Enhanced Sensitivity and Precision. *Plasmonics* **20**, 8781–8801 (2025).

57. Tene, T., Cevallos, Y., Vinueza-Naranjo, P. G., Inca, D. & Vacacela Gomez, C. Black Phosphorous-Based Surface Plasmon Resonance Biosensor for Malaria Diagnosis. *Sensors* **25**, (2025).

58. Singh, K., Shukla, S., Mishra, A. C., Lohia, P. & Dwivedi, D. K. Optimized prism-based surface plasmon resonance sensor for malaria detection: role of 2D nanomaterials for an enhancement in sensitivity and accuracy. *Microchimica Acta* **192**, (2025).

59. Singh, N. P., Mishra, A. C., Yadav, S., Lohia, P. & Dwivedi, D. K. Numerical analysis of SPR biosensor using zinc telluride, ferric oxide and black phosphorous for malaria detection. *Journal of Optics (India)* https://doi.org/10.1007/s12596-025-02460-w (2025) doi:10.1007/s12596-025-02460-w.

60. Tene, T. *et al.* Design and simulation of a graphene-integrated SPR biosensor for malaria detection. *Front. Bioeng. Biotechnol.* **13**, (2025).